OXFORD UNIVERSITY PRESS | Brain

Phospholipase A2 activating protein is associated with a novel form of Leukoencephalopathy

Journal:	*Brain*
Manuscript ID	BRAIN-2016-00581.R1
Manuscript Type:	Original Article
Date Submitted by the Author:	n/a
Complete List of Authors:	Falik-Zaccai, Tzipora; Galilee Medical Center; Faculty of Medicine in the Galilee, Bar Ilan University Savitzki, David; Galilee Medical Center Zivony-Elboum, Yifat; Galilee Medical Center Vilboux, Thierry; National Human Genome Research Institute, National Institutes of Health; Inova Translational Medicine Institute, Inova Health System Fitts, Eric; University of Texas Medical Branch at Galveston Shoval, Yishay; Galilee Medical Center Kalfon, Limor; Galilee Medical Center Samra, Nadra; Galilee Medical Center Keren, Zohar; Galilee Medical Center Gross, Bella; Galilee Medical Center; Faculty of Medicine in the Galilee, Bar Ilan University Chasnyk, Natalia; Galilee Medical Center Straussberg, Rachel; Schneider Children's Medical Center of Israel, Epilepsy Unit; Tel Aviv University Sackler Faculty of Medicine Mullikin, James; National Human Genome Research Institute, National Institutes of Health, NIH Intramural Sequencing Center (NISC) Teer, Jamie; H. Lee Moffitt Cancer Center Geiger, Dan; Technion Israel Institute of Technology, Computer Sciences Kornitzer, Daniel; Technion Israel Institute of Technology, Institute of Biomedical Sciences Bitterman-Deutsch, Ora; Galilee Medical Center; Faculty of Medicine in the Galilee, Bar Ilan University Samson, Abraham; Faculty of Medicine in the Galilee, Bar Ilan University Wakamiya, Maki; University of Texas Medical Branch at Galveston Peterson, Johnny; University of Texas Medical Branch at Galveston Kirtley, Michelle; University of Texas Medical Branch at Galveston Pinchuk, Iryna; University of Texas Medical Branch at Galveston Baze, Wallace; University of Texas MD Anderson Cancer Center Michale E Keeling Center for Comparative Medicine and Research Gahl, William; National Human Genome Research Institute, National Institutes of Health Kleta, Robert; UCL Institute of Child Health and Great Ormond Street Hospital NHS Trust Anikster, Yair; Edmond and Lily Safra Children\'s Hospital; Tel Aviv University Sackler Faculty of Medicine

	Chopra, Ashok; University of Texas Medical Branch at Galveston
Subject category:	Genetics
To search keyword list, use whole or part words followed by an *:	Genetics: neurodegeneration < GENETICS, Transgenic model < GENETICS, Whole-exome sequencing < GENETICS, Spasticity < MOVEMENT DISORDERS, Brain development < SYSTEMS/DEVELOPMENT/PHYSIOLOGY

Phospholipase A_2-activating protein is associated with a novel form of leukoencephalopathy

Tzipora C. Falik Zaccai MD[1,2], David Savitzki MD[3]*, Yifat Zivony-Elboum PhD[1]*, Thierry Vilboux PhD[4,5]*, Eric C. Fitts PhD[6]*, Yishay Shoval PhD[1], Limor Kalfon PhD[1], Nadra Samra MD[1], Zohar Keren PhD[1], Bella Gross MD[2,7], Natalia Chasnyk MD[1], Rachel Straussberg MD[8,9], James C Mullikin PhD[10,11], Jamie K. Teer PhD[12], Dan Geiger PhD[13], Daniel Kornitzer PhD[14] Ora Bitterman-Deutsch MD[2,15], Abraham O. Samson PhD[2], Maki Wakamiya PhD[16], Johnny W. Peterson PhD[6], Michelle L. Kirtley[6], Iryna V. Pinchuk, PhD[17], Wallace B. Baze DVM, PhD[18],William A Gahl MD PhD[4], Robert Kleta MD PhD[19], Yair Anikster MD PhD[9,20] , Ashok K. Chopra PhD, CSc[6]

[1]Institute of Human Genetics, Galilee Medical Center, Nahariya, Israel

[2] Faculty of Medicine in the Galilee, Bar Ilan University, Safed, Israel

[3]Pediatric Neurology Unit, Galilee Medical Center, Nahariya, Israel

[4]Section on Human Biochemical Genetics, Medical Genetics Branch, National Human Genome Research Institute, National Institutes of Health, Bethesda, MD, USA

[5]Division of Medical Genomics, Inova Translational Medicine Institute, Inova Health System, Falls Church, VA, USA

[6]Department of Microbiology & Immunology, University of Texas Medical Branch, Galveston, TX, USA

[7]Department of Neurology, Galilee Medical Center, Nahariya, Israel

[8]Pediatric Neurology Unit, Schneider Children's Medical Center, Petach Tikva, Israel

[9]Sackler School of Medicine, Tel Aviv University, Tel Aviv, Israel

[10]Comparative Genomics Analysis Unit, National Human Genome Research Institute, National Institutes of Health, Bethesda, MD, USA

[11]NIH Intramural Sequencing Center, National Human Genome Research Institute, Rockville, MD, USA

[12]Dept. of Biostatistics and Bioinformatics, H. Lee Moffitt Cancer Center, Tampa, FL, USA

[13]Computer Sciences, Technion - Israel Institute of Technology, Haifa, Israel

[14]Faculty of Medicine, Technion - I.I.T. and Rappaport Institute for Biomedical Research, Haifa, Israel

[15] Dermatology Clinic, Galilee Medical Center, Nahariya, Israel

[16]Transgenic Mouse Core Facility, Institute for Translational Sciences and Animal Resource Center, University of Texas Medical Branch, Galveston, TX, USA

[17]Department of Internal Medicine, University of Texas Medical Branch, Galveston, TX, USA

[18]Department of Veterinary Sciences, MD Anderson Cancer Center, Bastrop, TX, USA

[19]University College, Royal Free Hospital / UCL Medical School, London, UK

[20]Metabolic Disease Unit, Edmond and Lily Safra Children's Hospital, Sheba Medical Center, Tel Aviv, Israel.

*These authors contributed equally to this paper.

Running head: PLAA and progressive leukoencephalopathy

Corresponding author: Tzipora C. Falik-Zaccai, MD

Institute of Human Genetics, Galilee Medical Center

P.O. Box 21, Nahariya 22100. Israel

Tel: 972-50-7887-941; Fax: 972-4-9107553*; E-mail: falikmd.genetics@gmail.com*

Abstract

Leukoencephalopathies are a group of white matter disorders related to abnormal formation, maintenance, and turnover of myelin in the central nervous system. These disorders of the brain are categorized according to neuroradiological and pathophysiological criteria. Herein, we have identified a unique form of leukoencephalopathy in seven patients presenting at ages two to four months with progressive microcephaly, spastic quadriparesis, and global developmental delay. Clinical, metabolic, and imaging characterization of seven patients followed by homozygosity mapping and linkage analysis were performed. Next generation sequencing, bioinformatics, and segregation analyses followed, to determine a loss of function sequence variation in the phospholipase A_2-activating protein encoding gene. Expression and functional studies of the encoded protein were performed and included measurement of prostaglandin E2 and cytosolic phospholipase A_2 activity in membrane fractions of fibroblasts derived from patients and healthy controls. phospholipase A_2-activating protein -null mice were generated and prostaglandin E_2 levels were measured in different tissues. The novel phenotype of our patients segregated with a homozygous loss of function sequence variant, causing the substitution of Leucine at position 752 to Phenylalanine, in the phospholipase A_2-activating protein, which causes disruption of the protein's ability to induce prostaglandin E_2 and cytosolic phospholipase A_2 synthesis in patients' fibroblasts. *Plaa*-null mice were perinatal lethal with reduced brain levels of prostaglandin E_2. The non-functional phospholipase A_2-activating protein and the associated neurological phenotype, reported herein for the first time, join other complex phospholipid defects that cause leukoencephalopathies in humans, emphasizing the importance of this axis in white matter development and maintenance.

Keywords: Phospholipase A_2-activating protein; progressive leukoencephalopathy; autosomal recessive; startle response; complex phospholipid defects

Introduction

Leukoencephalopathies are brain white matter disorders categorized by neuroradiological and pathophysiological criteria (van der Knaap, 2001) into:

(a) Hypomyelinating diseases that are primary disturbances in myelin formation; Pelizaeus-Merzbacher disease may be considered the prototype of hypomyelinating disorders. Additionally, Pelizaeus-Merzbacher-like diseases phenotypically resemble Pelizaeus-Merzbacher disease but are inherited as autosomal-recessive disorders. Typically, no gene is identified, but in a small subset of Pelizaeus-Merzbacher-like diseases patients, sequence variations in *gap junction protein alpha 12*, coding for connexin 46.6 (Henneke et al., 2008; Uhlenberg et al., 2004), and sequence variations in the gene *HSPD1,* coding for heat shock 60-kDa protein 1, have been found (Magen *et al*., 2008). This group also includes syndromes in which hypomyelination is accompanied by other multi-organ involvements such as Cockayne's and Trichothiodystrophy Syndromes (Weidenheim *et al.*, 2009), and Oculodentodigital Dysplasia and 4H Syndrome (Atrouni *et al.*, 2003; Timmons *et al*., 2006).

(b) Dysmyelinating disorders with delayed and disturbed myelination, including most amino-acidopathies and organic acidurias. Since the brain (especially glial cells) is very sensitive to accumulation of toxic metabolites, secondary white matter abnormalities can be diagnosed in many metabolic disorders. Dysmyelination is also a main pattern of rare disorders such as SOX10-Associated Syndromes (the neurologic variant of Waardenburg-Shah Syndrome) (Pusch *et al*., 1998). Affected patients present a variable range of neurological symptoms: developmental delay, spasticity, ataxia, nystagmus, and in severe cases, profound neonatal hypotonia and congenital arthrogrypposis due to peripheral hypomyelination. 18q Deletion Syndrome, another example for disorders in this category, is characterized by neurological features such

as mental retardation, microcephaly, hypotonia, nystagmus and seizures, accompanied by additional multisystem defects, including partial growth hormone deficiency, facial, external ear, cardiac, and skeletal defects. Regions for dysmyelination, congenital aural atresia, and growth hormone insufficiency (18q22.3-q23) were identical and contained 5 known genes, including the myelin basic protein encoding gene. The dysmyelination region was 100% penetrant (Feenstra *et al.*, 2007).

(c) The third group is disorders with progressive demyelination, including "classic" leukodystrophies: X-linked adrenoleukodystrophy, Alexander's disease, Metachromatic leukodystrophy, Krabbe's disease, and disorders with white-matter vacuolisation such as Canavan's disease and Vanishing White Matter disease.

(d) Several leukoencephalopathies present with cystic degenerations, including megalencephalic leukoencephalopathy with subcortical cysts, first described by van der Knaap *et al.* in 1995 (van der Knaap *et al.*, 1995). Early-onset macrocephaly and delayed-onset neurologic deterioration, including cerebellar ataxia, spasticity, epilepsy, and mild cognitive decline, are characteristic features. Cystic leukoencephalopathy without megalencephaly has also been described (Henneke *et al.,* 2009).

(e) Disorders secondary to axonal damage include the autosomal recessive disorder giant axonal neuropathy**.** Patients present with progressive gait disturbances due to peripheral neuropathy, mental retardation, optic atrophy and spasticity; brain imaging studies show leukoencephalopathy. Pathological hallmarks of giant axonal neuropathy are axonal loss and axonal swellings filled with neurofilaments on nerve biopsy (Tazir *et al.*, 2009). Giant axonal neuropathy is caused by sequence variation in *GAN* encoding for gigaxonin, located on chromosome 16q24 (Bomont *et al.,* 2000).

Nevertheless, 50% of patients with leukoencephalopathies remain without specific diagnosis.

We report seven individuals from two consanguineous families presenting a unique phenotype of severe spastic quadriparesis, progressive microcephaly, thin corpus callosum, significant startle response, and severe global developmental delay. Genetic investigation revealed a novel missense variant in the phospholipase A_2-activating protein (*PLAA*) gene and disclosed a new mechanism required for normal development and maintenance of central nervous system white matter.

Methods

Patients

The Israeli Ministry of Health Ethics Committee for genetic experiments approved the proposed studies. Seven affected and twenty-three healthy individuals from two consanguineous families were enrolled in the study; they or their legal guardians provided written, informed consent. Clinical investigations included medical procedures, imaging and electrophysiological studies, and muscle biopsies. Skin biopsy was performed as part of the research protocol.

Molecular studies

Genetic Linkage Analysis

Linkage and haplotype analyses were performed as previously described (Zivony-Elboum *et al.*, 2012).

An analysis of 2050 polymorphic markers, spread across the genome at approximately 2cM intervals was performed for 9 family members. Statistical analysis of the logarithm of the odds (LOD) score was performed using the Pedtool-superlink tool. Areas with high LOD score were further examined using Linkage Mapping Set v2.5

HD5 kit and v2.5 MD10 (Applied Biosystems, Grand Island, NY) on 24 family members, according to the manufacturer's protocol.

Molecular Inversion Probes and Massively Parallel Sequencing

Molecular Inversion Probes were designed as described (Teer *et al.*, 2010) to cover the 2Mb of the candidate region (LC Sciences, Houston, TX). A total of 6498 amplimers had an average length of 433bp (+/-22bp). The amplimers covered 97% of the candidate region. DNA capture, library preparation, GAIIx sequencing (Illumina, San Diego, CA), and data analysis were performed as described (Teer *et al.*, 2010). Potential variants were filtered and visualized with VarSifter (Teer *et al*., 2012).

Sanger Sequencing

For dideoxy sequencing, primers were designed to cover the candidate sequence variations (primer sequences available upon request). Direct sequencing of the polymerase chain reaction (PCR) amplification products was performed using BigDye 3.1 Terminator chemistry (Applied Biosystems) and separated on an ABI 3130xl genetic analyzer (Applied Biosystems). Data were evaluated using Sequencher v5.0 software (Gene Codes Corporation, Ann Arbor, MI).

Molecular Modeling

Molecular modeling of the PLAA protein and assessment of the sequence variation impact was performed using the PyMOL Molecular Graphics System (Schrödinger, New York, NY) (Baugh *et al.,* 2011).

Expression analyses

Reverse Transcription of Full-Length PLAA Transcript

Primary fibroblasts [from healthy controls (n*PLAA*) and patients (m*PLAA*)] were harvested from one near-confluent 25 cm^2 flask and RNA extracted using the RNeasy mini kit (Qiagen, Valencia, CA). RNA samples were quantified using a Nanodrop

Spectrophotometer (Nanodrop Technologies, Wilmington, DE) and qualified by analysis on an RNA NanoChip using the Agilent 2100 Bioanalyzer (Agilent Technologies, Santa Clara, CA). Synthesis of complimentary DNA (cDNA) was performed using the Taqman Reverse Transcription Reagents Kit (Applied Biosystems). The reaction conditions were as follow: 10 min at 25ºC; 30 min at 48ºC; and 5 min at 95ºC. PCR amplifications of cDNA were performed using FailSafe buffer C (Epicenter Biotechnologies, Madison, WI) with *PLAA* primers 5'CGAGCGGCGCAACCAGGTACC3' and 5'GCATTCACTTACTTTAGCTGGTTCTG3' at a final concentration of 1 µM. Thermal conditions for 40 cycles of PCR were as follow: 94ºC for 30 sec, 60ºC for 30 sec, and 68ºC for 7 min.

Real Time (RT)-quantitative (q)PCR

One µg of RNA extracted from fibroblasts from healthy controls and patients was subjected to cDNA synthesis followed by RT-qPCR using the iTaq Universal SYBR Green mix (Bio-Rad, Hercules, CA). The final concentration of the *PLAA* primers (5'GACT TGGGAATCCC AGCTTTTC3' and 5'TTCCCATACTTGCAGAACCTG3'; Accession # NM_001031689) was 300 nM. RT-qPCR assays were performed with human 18S RNA, glyceraldehyde 3-phosphate dehydrogenase (GAPDH), L19 ribosomal protein, and polymerase beta (PolB) as housekeeping protein encoding genes to normalize *PLAA* transcript levels. Absolute analysis was performed using known amounts of a synthetic transcript of the gene of interest. All RT-qPCR assays were run on the ABI Prism 7500 Sequence Detection System and the conditions were as follow: 50^{o}C for 2 min, 95^{o}C for 10 min, and then 40 cycles of 95^{o}C for 15 sec and 60^{o}C for 1 min. The results shown were the averages and standard deviations from three independent experiments performed in triplicate.

The pro-inflammatory gene expression in fibroblasts with n*PLAA* or the m*PLAA* gene was carried out using the appropriate assays-on-demand™ gene expression assay mix consisting of a 20X mix of unlabeled PCR primers and TaqMan® MGB probe, FAMTM dye-labeled (Life Science Technology Inc, CA). Human GADPH, β-actin, and 18S RNA encoding genes were used to normalize transcripts for various cytokines. The primer sequences for various cytokine genes are available upon request. The reactions were carried out according to the manufacturer's instruction using a Bio-Rad Q5 RT-qPCR machine. The results shown were the averages and standard deviations from three independent experiments performed in triplicate.

Western blot analysis

β-catenin. Briefly, 70 µg of protein samples from healthy controls' and patients' fibroblasts with or without lipopolysaccharide [LPS; 10 µg/mL] stimulation) were electrophoresed on 4-20% Mini-Protean TGX Pre-cast Tris/Glycine gels (Bio-Rad) and then transferred to nitrocellulose membranes. The membranes were probed with non-phospho (active) β-catenin (Cell Signaling Technology, Danvers, MA) and β-Tubulin (Santa Cruz) antibodies as described by the manufacturer. An anti-rabbit horseradish peroxidase conjugated secondary antibody (Southern Biotech, Birmingham, AL) was then added, and proteins detected by using enhanced chemiluminescence with Super Signal West Femto Maximum Sensitivity substrate (Thermo Scientific). The membranes were then imaged with GE ImageQuant LAS 4000 (General Electric, Fairfield, CT).

Biochemical studies

Measurement of Prostaglandin E2 (PGE_2)

Primary human fibroblasts from healthy controls and patients were grown in Dulbecco modified essential medium with 15% fetal bovine serum at 37°C and 5% CO_2. Fibroblasts from patients and control subjects were treated with 10 μg/mL LPS or cholera toxin for 24 hours; and the cell culture supernatants were collected. PGE_2 levels were determined using enzyme immunoassay kit (Cayman Chemicals, Ann Arbor, MI). To examine PGE_2 levels in mouse tissues, samples were subjected to solid phase extraction on C_{18} columns (Cayman Chemicals) prior to measurements.

Preparation of Membrane Fractions from Fibroblasts

Membrane fractions from healthy controls and patients' unstimulated and LPS-stimulated fibroblasts were isolated using established procedures (Zhang *et al.,* 2008). Protein concentrations in membrane fractions were determined using Bradford Protein Reagent (Bio-Rad).

Measurement of Cytosolic Phospholipase A_2 ($cPLA_2$) Activity

The $cPLA_2$ activity in membrane fractions of fibroblasts from patients and healthy controls) was determined using PLA_2 activity kit (Cayman Chemicals). The enzymatic activity was normalized to protein concentration for each sample. Bee Venom PLA_2 was used as a positive control.

Complementation studies

Fibroblasts from patients (*mPLAA*) or healthy controls (*nPLAA*) were grown and electroporated with the recombinant plasmid or the vector alone using Lonza Nucleofector and Human Dermal Fibroblast kit (Lonza, Basel, Switzerland). The m*PLAA* fibroblasts were electroporated with either CMV promoter-based pIRES2-DsRed2-*nPLAA* for complementation or pIRES2-DsRed2 vector (Clontech, Mountain View, CA) alone as a control. n*PLAA* fibroblasts were also electroporated with the vector alone to serve as an additional control.

Mouse model

All animal experiments were performed at the University of Texas Medical Branch. Animals were housed in a specific-pathogen free facility at a constant temperature (68-79^{o}F) and humidity (30-70%) on a 12 hours light-dark cycle. Autoclaved water and irradiated feed were given to the animals *ad libitum*. All procedures were performed in accordance with the protocol reviewed and approved by University of Texas Medical Branch Institutional Animal Care and Use Committee, and in compliance with the institutional policies/guidelines and the Guide for the Care and Use of Laboratory Animals, 8th edition. Euthanasia methods used in the procedures were consistent with the American Veterinary Medical Association Guidelines for the Euthanasia of Animals, 2013 edition. Generation of *Plaa*-null mice (*Plaa* gene targeting) and genotyping of the mice have been described in Supplemetary Materials and Methods section.

Preparation of Mouse Tissue Samples for PGE_2 Measurements

In brief, mouse tissues were suspended in homogenization buffer (0.1M disodium phosphate buffer, pH 7.4, 1 mM EDTA, 10 µM indomethacin) and sonicated. Samples were normalized by measuring protein concentrations using the Bradford Protein Reagent (Bio-Rad). After homogenization, 4 volumes of ethanol were added and samples centrifuged at 3000 x *g* for 10 min at 4°C. Supernatants were collected and ethanol removed by vacuum centrifugation before acidification of the samples with 1M acetate buffer. The samples were then loaded on pre-washed C_{18} cartridges, washed with H_2O, and eluted with ethyl acetate and 1% methanol (99:1 v/v). Ethyl acetate was removed by vacuum centrifugation and samples reconstituted in PGE_2 assay buffer for measuring PGE_2.

Histopathology

Sections (5 µm) representing skin, lungs, and the brain cerebral cortex from embryonic day (E) 18.5 mouse embryos were fixed in 10% neutral buffered formalin. The tissue sections were mounted on slides and stained with hematoxylin and eosin. The histopathological evaluation of the tissue sections was performed in a blinded fashion.

Statistical analysis

Where appropriate, at least three independent experiments were performed in triplicate and data analyzed using one-way ANOVA with Tukey or Tukey *post-hoc* correction.

Results

Patients

Seven individuals from two families, all products of consanguineous marriages and uneventful pregnancies, presented with progressive leukoencephalopathy (**Figure 1A&B**), defined as dysmyelinating according to the known categories of Van der Knaap and his colleagues (van der Knaap, 2001). Affected individuals were normal at birth, with onset of neurological symptoms at age 2-4 months (**Table 1**). Symptoms included spasticity of lower limbs rapidly progressing to upper extremities, resulting in severe quadriparesis with symptoms of corticospinal tract impairment and posture deformation. Involvement of extrapyramidal system function included dystonic posturing, rigidity/freezing, and hypomimia/amimia. All patients suffered from severe mental and language developmental delay. The motor functions were also prominently impaired (level V, according to Gross Motor Function Classification System (Palisano et al., 1997). Abnormally exaggerated startle reflex to an auditory stimulus was observed in 6 patients, and seizures developed in three.

Head circumferences, normal at birth, decreased to more than 2 standard deviation below the mean in the ensuing years. In two patients, we observed an unexplained gradual increase in Head circumferences up to 75% after the age of approximately 5 years. Weight and height, also normal at birth, fell to 3-4 SD below mean in 5 patients but returned to 50-75% in two out of five patients. Progressive chest deformities (kyphosis/pectus carinatum) were observed in all patients. Additional phenotypic characteristics included contractures of large joints, hyperextensibility of small ones, rocker bottom feet, hypertrichosis, and hyperhidrosis of palms and feet (**Figure 1C, a-d**).

Brain MRI demonstrated radiological signs of periventricular and subcortical damage including delayed myelination and atrophy, which worsened with age as a result of enlargement of ventricular system. Thin corpus callosum was a prominent feature in all of the patients. In one case, periventricular lesions were observed (Figure 1D). Muscle biopsy in patient VI_3 showed normal oxidative phosphorylation and increased aggregation of collagen.

Molecular analyses

Molecular Studies

Linkage analysis, performed on 24 individuals from family I, identified a 1.9Mb region between markers D9S265 and rs1330920 with a maximal LOD score of 3.24 at D9S1121; the region contained 11 genes (**Figure 2A&B**). Seven samples were sequenced (two affected, 2 obligate carriers, and 3 unaffected individuals from the same village) with an average coverage of 82 ± 2% (all coding regions were covered). Haplotype analysis (D9S259-D9S169) supported a common ancestral haplotype in families A and B (**Table S1).**

Next Generation Sequencing

A total of 4289 variants were identified, but only four of them affected protein sequences (**Table S2**). Out of these four variants, only one was present in a homozygous state in the affected individuals and in a heterozygous state in the obligate carriers. The three others were identified in the samples of unaffected individuals. The missense variant, NM_001031689.2: c.2254C>T (p.Leu752Phe); was confirmed by Sanger sequencing (**Figure 2C**) in all affected individuals and obligate carriers. All seven affected individuals were homozygous for this sequence variation; all their parents were heterozygous.

The above PLAA variant (p.Leu752Phe) was neither observed in the Exome Aggregation Consortium (60.706 unrelated individuals, Exome Aggregation Consortium [ExAC], Cambridge, MA, http://exac.broadinstitute.org/, accessed February 2016) nor in the NHLBI database (6,500 unrelated individuals, Exome Variant Server, NHLBI GO Exome Sequencing Project, Seattle, WA [URL: http://evs.gs.washington.edu/EVS/] accessed February 2016). Population screening of 92 healthy village residents revealed 3 carriers of this sequence variation (prevalence 3.3%).

The leucine at position 752 in PLAA is highly conserved through *Saccharomyces cerevisiae* (**Figure 2D**), with the exclusion of Zebrafish (threonine) and *Caenorhabditis elegans* (valine). This amino acid substitution is predicted to be deleterious by SIFT (Score: 0.04) (http://sift.jcvi.org/www/SIFT_aligned_seqs_submit.html) and probably damaging by PolyPhen-2 (Score 0.983) (http://genetics.bwh.harvard.edu/pph2/index.shtml).

Structural Effects of p.Leu752Phe substitution in PLAA

The structure of PLAA PUL domain, in which Leu752 resides, was recently determined with atomic resolution (Qiu *et al.*, 2010). PUL domain consists of 15 tightly packed α-helices forming a 6-mer Armadillo domain. This protein fold consists of tightly packed helices in a single rigid structure found in several proteins such as importin-α, β-catenins, and Hsp70 binding protein (Hatzfeld, 1999). The Armadillo domain of PLAA is held together mainly through conserved leucine residues that zip together adjacent α-helices. On average, leucine is present every 3-4 residues, corresponding to one turn of the helical wheel. Such Armadillo repeats form banana-shaped domains that generate good binding surfaces, particularly on the inside curvature (Hatzfeld, 1999).

In PLAA, the putative binding site is also paved with conserved residue (Sievers *et al.*, 2011). Based on these data, p.Leu752Phe mutation appears to disrupt the tightly packed leucine network of the PLAA PUL domain and deform the banana-like binding surface (**Figure 2E**).

Expression studies

PLAA mRNA Expression

At the transcriptional level, fibroblasts from patients were capable of expressing full length *PLAA* transcript similar to that of n*PLAA* fibroblasts **(Figure 3A)**. Furthermore, based on RT-qPCR, no difference in the levels of *PLAA* transcript was noted between n*PLAA* versus m*PLAA* fibroblasts **(Figure 3B)**. As amino acid changes can have unexpected effects on protein stability, we sought to confirm production of PLAA protein in fibroblasts with and without the defined mutation in the *PLAA* gene. Confocal microscopy was performed to localize PLAA in normal and patient fibroblasts. All patient fibroblasts tested showed some localization of PLAA in the nucleus and majority of PLAA in the cytoplasm, which were similar in levels found in the fibroblasts of healthy controls (**Figure 3C&D**).

Functional Effects of p.Leu752Phe on PLAA

Previous studies showed that PLAA loss causes severe ubiquitin depletion, accumulation of misfolded proteins, and impaired cellular survival, in *S. cerevisiae* (Mullally et al., 2006; Qiu et al., 2010). However, these effets were neither shown in the growth *of S. cerevisiae* and its Δ*DOA1* (an ortholog of human *PLAA* in yeast) mutant nor on ubiquitin depletion in fibroblasts from healthy controls versus patients. (See methods and results in the supplementary section.) Consequently, we examined other known functions of the PLAA protein. PLAA induces PGE_2 production by

increasing levels of PLA_2 and cyclooxygenase (COX)-2 proteins, two major regulators of prostaglandins (Calignano *et al.*, 1991; Zhang *et al.*, 2008).

Investigating this function, we measured PGE_2 levels in our patients' fibroblasts. Healthy, unstimulated cells expressing n*PLAA* exhibited ~2-fold higher levels of PGE_2 compared to patients' fibroblasts (**Figure 4A black bars**); this difference became much more prominent after LPS and cholera toxin treatment of the cultured n*PLAA* cells (~5000-fold [light gray bars] and ~1000-fold [dark gray bars], respectively). LPS treatment induced $cPLA_2$ activity in normal fibroblasts, but did not elicit a similar response in patients' cells (**Figure 4B**). These results suggest that p.Leu752Phe in PLAA abrogates its ability to induce prostaglandin biogenesis and properly respond to related stresses. Finally, transfection with a plasmid expressing n*PLAA* rescued PGE_2 levels and $cPLA_2$ activity in both untreated and LPS-stimulated patients' fibroblasts (**Figure 4C&D**).

We previously observed that PLAA regulates NF-κB-mediated inflammatory responses, and in particular inducible interleukin (IL)-6 (Zhang *et al*., 2008). Herein, we observed that p.Leu752Phe variation in PLAA abrogated expression of LPS induced IL-6, IL-8, and macrophage migration inhibitory factor (MIF) expression in patient fibroblasts when compared to fibroblasts from a representative healthy control based on RT-qPCR (**Figure 4E-G**).

Cell Biology studies

NF-κB Recruitment to the Nucleus is Unaffected by p.Leu752Phe in the PLAA.

We investigated the NF-κB signaling pathway which is known to be regulated by PLAA (Zhang et al., 2008) and show it is intact in both fibroblasts from patients and healthy controls (Figure S1A&B). For detailed methods, results and figure see the suplementary section.

β-catenin wingless integration (Wnt) Signaling is Not Affected by p.Leu752Phe PLAA

We investigated Wnt signaling by examining levels of non-phospho (active) β-catenin in n*PLAA* versus m*PLAA* fibroblasts with and without LPS stimulation. As shown in **Figure S1C**, the levels of active β-catenin were increased after LPS stimulation to a similar extent in both types of fibroblasts. Detailed results are summarized in the supplimentary section.

Mouse model

Inactivation of the Plaa Gene Results in Perinatal Lethality in Mice

We generated *Plaa*-null mice using gene targeting technology (**Figure S2**). While heterozygous (*Plaa*$^{+/-}$) mutants were viable and fertile, the homozygous (*Plaa*$^{-/-}$) mutants exhibited perinatal lethality. Initially we genotyped 66 pups derived from heterozygous intercrosses, typically on postnatal day 4-9. Twenty-eight pups were wild-type, thirty-eight were *Plaa*$^{+/-}$, and there was no *Plaa*$^{-/-}$ mutant. To determine when the *Plaa*-null mice died, we set up timed heterozygous intercross mating and examined embryos at different time points (**Table S3**). At E14.5, we recovered live, overtly normal *Plaa*$^{-/-}$ embryos, which were indistinquishable from *Plaa*$^{+/-}$ or wild-type littermates. At E18.5, we found mostly live (with a beating heart) but some dead *Plaa*$^{-/-}$ embryos. *Plaa*$^{-/-}$ embryos were grossly normal but smaller than *Plaa*$^{+/-}$ or wild-type littermates. The average body weights of live *Plaa*$^{-/-}$, *Plaa*$^{+/-}$, and wild-type embryos were 0.83 ± 0.11 g (n=14), 1.03 ± 0.17 g (n=32), and 1.34 ± 0.14 (n=9) at E18.5, respectively. While differences in weights between wild-type and *Plaa*$^{+/-}$ were not statisitcally significant, weight differences between wild-type and *Plaa*$^{-/-}$ ($\leq$0.0001) and *Plaa*$^{-/-}$ and *Plaa*$^{+/-}$ ($\leq$0.001) were significant by one way ANOVA with Tukey *post hoc* correction.

Gross examination revealed that all of the near-term *Plaa*$^{-/-}$ embryos had abnormal or underdeveloped spleens, which were transparent/pale and smaller. Interestingly, we also found one embryo with exencephaly/microcephaly among a total of 41 *Plaa*$^{-/-}$ embryos examined. We attempted to resuscitate some of the E18.5 embryos, but *Plaa*$^{-/-}$ embryos could not be resuscitated. While *Plaa*$^{+/-}$ and wild-type embryos reacted to the pinch and started gasping for air, *Plaa*$^{-/-}$ embryos did not make any voluntary or involuntary movement. Subsequently, we also found five *Plaa*$^{-/-}$ neonates that were naturally delivered, but they were all found dead. Notably, one of the dead *Plaa*$^{-/-}$ neonates had posterior truncation. The dead *Plaa*$^{-/-}$ neonates appeared to have no air in their lungs. To date, we have not found any live *Plaa*$^{-/-}$ neonate. These observations suggest that *Plaa*-null mice likely died shortly before or after birth.

A Tissue-Specific PGE_2 Reduction and Perinatal Lethality of Plaa-Null Mice

To validate the results observed for the human fibroblasts carrying m*PLAA*, we evaluated the levels of PGE_2 in wild-type, *Plaa*$^{+/-}$, and *Plaa*$^{-/-}$ embryos. We isolated lungs, brain, liver, and heart tissues from E18.5 embryos, and determined PGE_2 levels for each organ individually (**Figure 5A-D**). In the brain, there was a gene copy dependent reduction of PGE_2 with significant reduction in *Plaa*$^{+/-}$ embryos compared to wild-type ($p<0.001$) as well as a significant decreased level of PGE_2 in *Plaa*$^{-/-}$ compared to *Plaa*$^{+/-}$ ($p<0.05$) embryos (**Figure 5B**). PGE_2 levels were significantly decreased in *Plaa*$^{-/-}$ lungs, and *Plaa*$^{+/-}$ and *Plaa*$^{-/-}$ hearts, but not in the liver (**Figure 5A,C&D**). It is unclear why gene copy dependent reduction of PGE_2 was noted in some organs but not in others.

Histopathological Analysis of Skin, Lungs, and Brain Cerebral Cortex of Plaa-Null Mice

As shown in **Figure 6A**, lungs from WT mice embryos exhibited the presence of organized alveolar spaces and thin alveolar walls. However, embryos from *Plaa*$^{+/-}$ and *Plaa*$^{-/-}$ mice showed progressively unorganized alveolar spaces and thickening of the alveolar walls, suggesting underdeveloped or immature lungs.

In the brain cerebral cortex of wild type embryos, the neurons showed large nuclei and were fully matured, with no indication of degeneration. No signs of apoptotic bodies were noted. There were a few round dark cells that represented either oligodendroglia or granular immature neurons (**Figure 6B**). The *Plaa*$^{+/-}$ embryos had smaller neuronal nuclei and about the same density of the round dark cells. On the contrary, *Plaa*$^{-/-}$ embryos had a vast area of neurons with smaller dark-stained round nuclei that could be described generally as "more granular" in type, an indication of less maturity and differentiation. No significant differences were observed in the skin of wild type versus mutant mouse embryos (**Figure 6C**). Typical tissue sections representing multiple fields and from 2-4 embryos are shown.

Discussion

PLAA is a regulatory molecule implicated in modulating production of host cell phospholipases (e.g., PLA_2) (Clark *et al.*, 1991; Ribardo *et al.*, 2002). Induction of PLA_2 is highly regulated by mitogen-activated protein kinases and NF-κB (Zhang *et al.*, 2008). PLA_2 hydrolyzes membrane phospholipids to produce arachidonic acid, which is used as a substrate to produce prostaglandins and leukotrienes (eicosanoids) through cyclooxygenase and lipoxygenase pathways, respectively (Ribardo *et al.*, 2002).

In this report, we present seven patients from two families with severe, unique, progressive leukoencephalopathy. Based on the clinical and radiological findings, these patients could be categorized into the group of primary delay in myelin

formation and disturbed myelination (van der Knaap, 2001). Brain biopsies were not performed and histopathological data are not available to confirm or rule out our clinical impression.

All patients are homozygous for a founder sequence variant (p.Leu752Phe) in *PLAA*. that did not lead to the production of unstable transcript or protein.

The PLAA protein is composed of three major domains: N' terminal, multi-protein complex assembly domain contains 7 WD40 repeats; central PFU domain includes a ubiquitin binding region and an SH3 region; and C' terminal PUL domain consists of 6 Armadillo repeats and binds to valosin-containing protein, also known as Cdc48 and p97 (Qiu et al., 2010). Our results suggest that the p.Leu752Phe sequence variant disrupts the protein's Armadillo domain, possibly impairing cells' ability to induce prostaglandin production through a non-NF-κB signaling pathway.

Armadillo folds such as those found in PLAA, importin-α, and β-catenins, play a role in central nervous system development in *Drosophila*. Specifically, disruption of cell-cell adhesion function of Armadillo results in construction defects of the axonal scaffold (Loureiro and Peifer, 1998). Interestingly, a recent study suggested that $PLA_2α$ regulates the Wnt/β-catenin pathway (Han *et al.*, 2008), which is implicated in neurogenesis, central nervous system morphogenesis, hirsutism, sweat gland morphology, short tendons, and kyphosis (Haara et al., 2011 ; Joksimovic and Awatramani, 2014; Toribio et al., 2010; Zhang et al., 2014). In this pathway, β-catenins transduce Wnt signals during embryonic development. Therefore, we hypothesized that PLAA, which activates PLA_2, indirectly regulates the Wnt/β-catenin pathway, accounting for the pathology seen in our patients. However, our data indicate that the p.Leu752Phe in *PLAA* found in our patients did not alter Wnt signaling.

Experimentally, activation of PLAA was recently shown to occur *via* 1α,25(OH)$_2$D3 binding to a specific membrane-associated receptor, Pdia3, in caveolae, regulating growth zone chondrocytes (Doroudi *et al.*, 2014). These findings might explain non-neurological features of progressive chest deformities (kyphosis/pectus carinatum) present in affected individuals.

Complex phospholipid defects involving the central nernous system have received much attention of late (Lamari *et al.,* 2013), providing insights into late-onset neurodegenerative disease pathophysiology, such as gene *PLA2G6* encoding PLA$_2$, underlying AR infantile neuroaxonal dystrophy, neurodegeneration associated with brain iron accumulation, and early-onset dystonia/parkinsonism (Gregory et al., 2008; Khateeb et al., 2006).

Furthermore, PGE$_2$ plays a dual role, both neurotoxic and neuroprotective, in the brain and nervous system, a role modulated by its four receptors (Milatovic *et al.*, 2011). Different binding affinities, varying cellular expression profiles, and attenuation of secondary messengers of these receptors lead to intricate, and sometimes opposing, signal transduction. While in Alzheimer's disease and amyotrophic lateral sclerosis it plays a neurotoxic role (Bazan *et al.*, 2002), in excitotoxicity and cerebral ischemia scenarios, PGE$_2$ is neuroprotective (Gregory *et al.,* 2008). Thus, modulation of PGE$_2$ appears critical for neurological function. When PGE$_2$ levels are reduced by deficiency of synthetic enzymes PLA$_2$ (Gregory *et al.,* 2008), COX-1 and COX-2 (FitzGerald, 2003) or PGE$_2$ receptor (EP1-4), neurological impairment might occur.

Mohri and colleagues (Mohri *et al*., 2006) have described prostaglandins as neuroinflammatory molecules that heighten pathological response to demyelination in twitchier mice. Similarly, the arachidonic acid pathway was shown to be modulated during cuprizone neurotoxin induced-demyelination and remyelination processes

(Palumbo *et al.*, 2011). Altogether, these data support a causative relationship between abnormal PLAA activity and the severe leukoencephalopathy seen in our patients.

Of special interest is the prominent feature seen in six patients of exaggerated startle response, previously linked to dysmyelination/hypomyelination disorders, such as multiple sclerosis (MS). In 1978, Mertin and Stackpoole showed that treatment with essential fatty acids, including arachidonic acid, suppresses experimental autoimmune encephalomyelitis in rats, and isabolished by inhibition of prostaglandin biosynthesis (Mertin and Stackpoole, 1978). Additionally, decreased inhibition of startle generator structure was reported to be associated with MS (Ruprecht *et al.*, 2002). The calcium-independent PLA_2 inhibitor was also linked to reduced pre-pulse inhibition of acoustic startle reflex in other studies (Lee *et al.*, 2009).

Multiple studies link PGE_2 and arachidonic acid pathways to neurodegenerative disorders, but their exact roles in causing white matter disorders remain unclear. We hypothesize that the prominent startle reflex dys-inhibition in our patients may be related to brainstem lesions as part of the diffused axonal and myelin damage.

Additional interesting observation was that p.Leu752Phe substitution in PLAA results inability of the patient fibroblasts to induce IL-6, IL-8, and MIF in response to the NF-κB activating molecule LPS. While the pathophysiological relevance of this observation is yet to be determined, an association between neurodegenerative disorders and inflammatory cytokine responses has been suggested recently (Schmitz et al., 2015). These cytokines are known for their pleiotropic function and are implicated in activation of microglia, proliferation, migration, and homing of different immune and non-immune cells. In addition, PGE_2 has been shown to be important leading to increased production of IL-6 and IL-8(Cho et al., 2014). Thus, taken

together, our observation may suggest that the pathogenesis of the leukoencephalopathy linked to the p.Leu752Phe subbstitution in PLAA implicates inability to mount appropriate inflammatory responses during pre-/post-neonatal development.

The phenotype of our patients, homozygous for p.Leu752Phe in *PLAA* and with reduced $cPLA_2$ activity and PGE_2 levels, adds new insights into this axis and its role in leukoencephalopathic disorders' pathogenesis.

Knockout mouse data provide a clue into potential disease mechanisms seen in the patients described in this paper. The disturbance in prostaglandin signaling results in a variety of pathological conditions. PLAA-deficient mice showed some phenotypes, specifically perinatal death, immature lungs with reduced PGE_2, and reduced body weight similar to that of *Ptgs1* (Cox-1)-*Ptgs2* (Cox-2) double knockouts (Yu *et al.,* 2006) and *Ptgs3* knockouts (Nakatani *et al.,* 2007). The double mutants, as well as *Ptgs4* knockouts (Nguyen *et al.*, 1997) died perinatally due topatent ductus arteriosus, *Ptgs3* knockouts showed perinatal death, possessed immature lungs, and PGE_2 levels were markedly decreased in the organ. The mutants also exhibited decreased body weight and skin morphological and physiological defects. Additionally, prostaglandin signaling is implicated for its roles in a range of physiologicalprocesses such as cell fate decision (Nissim *et al.,* 2014), cell differentiation (Li *et al.,* 2000), and ciliogenesis (Jin *et al.,* 2014). The inability of *Plaa*-null mice to survive, which may stem from impaired neuronal development in the brain, together with our findings that PGE_2 levels were significantly reduced in the brain and the lung of *Plaa*-null mouse embryos, raise the possibility that the pathogenesis of the condition we observed in PLAA-deficient mice and in patients with a non-functional PLAA could be a developmental defect caused at least partly by ineffective prostaglandin signaling.

Clearly, the *Plaa*-null mouse model provides an important tool to study the role of PLAA in central nervous system development and maintenance. Creating *Plaa* conditional knockout mice or *Plaa* knock-in mice carrying the p.Leu752Phe sequence variant would enable us to perform more detailed histopathological studies of the brain and thus to learn what type of leukoencephalopathy is caused by the *PLAA* sequence variant described here or by PLAA deficiency. Such an animal model would further contribute to the understanding of the significant role of arachidonic acid and PGE_2 pathway in the normal development and maintenance of the brain.

In conclusion, we have presented a cohort of patients with progressive microcephaly and leukoencephalopathy, providing the first documentation of a PLAA-related disease. Although the interplay between PLAA, the abnormal production of PGE_2, and the resultant hypo-myelination has not been thoroughly delineated, our data clearly indicated an association of this axis with brain development. Supportive evidence from the literature and improved understanding of the new players in this pathway should lead to new therapeutic avenues for intervention in both rare autosomal recessive disorders and late onset common diseases that involve reduced central nervous system white matter.

Acknowledgments

We thank the families who participated in this study and the physicians and nurses who helped in the care for these patients. Special thanks to Dr. Sarah Amit who cared for these patients in Galilee Medical Center's Child Development Unit and referred them to our attention. Tragically, Dr. Amit passed away during this study. We would like to thank Dr. Raya Rod and Dr. Assnat Blum of GMC's Child Development Unit for performing neurological and clinical work-up on the patients, and Dr. Tatiana Freidman who participated in clinical follow-up of patients.

We thank the Exome Aggregation Consortium and the groups that provided exome variant data for comparison.

Sequencing of the Molecular Inversion Probe was performed by the NIH Intramural Sequencing Center.

We thank Dr. Benjamin B. Gelman, Department of Pathology, UTMB, in interpreting some of the brain slide pictures.

We thank Ms. Tobie Kuritsky for English editing and technical assistance in handling the submission process.

Funding

This Study was funded by the Rappaport Institute for Research (to TFZ) by the Rappaport Faculty of Medicine, Technion, Haifa, and by the "Izvonot" foundation of the Israeli Ministry of Justice (to TFZ), Jerusalem, Israel.

This research was supported by the Intramural Research Program of the National Human Genome Research Institute, National Institutes of Health, Bethesda, Maryland, USA.

Funding made available through the endowments of Leon Bromberg Professorship for Excellence in Teaching and Robert E. Shope MD and John S Dunn Distinguished Chair in Global Health to AKC is greatly acknowledged.

Author Contributions to the Study and Manuscript

Tzipora C. Falik Zaccai initiated the project, was principal investigator, recruited the patients and families, designed the experiments, and wrote the manuscript.

David Savitzki performed neurological and clinical work up on the patients and followed them. He participated in preparing the manuscript.

Yifat Zivony-Elboum performed DNA linkage analyses and sequencing studies.

Thierry Vilboux performed NGS studies and expression analyses, and participated in writing the manuscript.

Yishay Shoval performed sequencing studies, bioinformatics analyses, yeast studies, and participated in writing the manuscript

Limor Kalfon performed sequencing studies, tissue cultures and haplotype analyses, and participated in writing and editing the manuscript

Nadra Samra performed neurological and clinical work up on the patients and participated in preparing the manuscript.

Zohar Keren performed sequencing studies and segregation analyses.

Bella Gross performed neurological and clinical work up on the patients and participated in preparing the manuscript.

Natalia Chesnik performed neurological and clinical work up on the patients and participated in preparing the manuscript.

Rachel Straussberg performed neurological and clinical follow up on the patients.

James C Mullikin participated in the NGS studies.

Jamie K. Teer participated in the NGS studies.

Dan Geiger performed the bioinformatics related to linkage analysis.

Daniel Kornitzer participated in the yeast studies.

Ora Bitterman-Deutsch participated in establishing fibroblasts tissue cultures of the patients.

Abraham O. Samson participated in the bioinformatics analysis of the protein in native and mutation state.

William A Gahl contributed to NGS studies, and participated in writing and editing the manuscript.

Robert Kleta contributed to linkage and segregation analyses, and participated in writing the manuscript.

Yair Anikster participated in NGS studies and expression analyses, and participated in writing the manuscript.

Eric C. Fitts performed biochemical and microscopic studies, conducted data analysis, and contributed to the writing of the manuscript

Maki Wakamiya developed and maintained transgenic mouse lines and obtained mouse tissues for analysis.

Johnny W. Peterson interpreted data and participated in manuscript writing and editing.

Michelle L. Kirtley helped in maintaining fibroblasts, isolating RNA, and performing Western blot analysis.

Iryna V. Pinchuk performed experiments related to cytokine levels in fibroblasts and wrote portion of the manuscript.

Wallace B. Baze performed histopathological studies on mouse tissues.

Ashok K. Chopra designed the experiments, interpreted the data, and participated in writing and editing of the manuscript.

Potential Conflicts of Interest: None

Table 1. Clinical characteristics of patients: Data were collected regarding medical history, metabolic measurements, imaging, electrophysiological studies and muscle biopsy. Complete physical, neurological, and developmental examinations were performed on seven patients. The disease phenotype in all patients was similarly severe. NA=Not Available. MRI= Magnetic Resonance Imaging. SSEP= Somatosensory Evoked Potentials.

Patient	A(VI_3)	A(VI_4)	A(VI_5)	A(V_6)	A(VI_{10})	B(IV_2)	A(VI_1)
Sex	F	F	M	M	M	M	M
Age (y)	15	11	16	34	5	3	2
AO (m)	4	4	3	4	3	2	3
FTT	+++	+	+++	+++	++	+++	+++
Progressive microcephaly	+++	+	+++(*)	*+	+	+++	+
Pyramidal Signs Lower extremities	+++ (plegia) Babinski sign	+++ Babinski sign	+++ Babinski sign, Clonus	+++ Babinski sign	+++ Babinski sign	++	+++
Pyramidal Signs Upper extremities	++	++	++	++	++	++	+++
Extra-pyramidal Signs	++	++	+++	+++	++	+++	+++
GMFCS (Level)	V	V	V	V	V	V	V
Cognitive and Language Development	Severe	Severe	Severe	Severe	Severe	Severe	Severe

Patient	$A(VI_3)$	$A(VI_4)$	$A(VI_5)$	$A(V_6)$	$A(VI_{10})$	$B(IV_2)$	$A(VI_1)$
Delay							
Exaggerated Startle Response	+	+	+	NA	+	+	+
Seizures	-	-	+	+	-	+	-
MRI/CT of brain	Reduce mass of white matter. Thin Corpus Callosum Delayed Myelination (especially along Cortico-Spinal tract and posterior Genu of Capsula Interna (at age 13m) Worsening of brain atrophy at the age of 3 2/12. Sparing of basal ganglia.	Enlargement of ventricular system Thin Corpus Callosum Normal MRI of spinal cord (at age 1y)	White matter atrophy with periventricular lesions resemble PVL Thin Corpus Callosum (at age 2y)	Severe general and especially white matter atrophy and thin Corpus Callosum (at age 30y	White matter atrophy, periventricular and subcortical lesions Thin Corpus Callosum Enlargement of ventricular system (at age 1y 9m)	Delayed myelination. Thin Corpus Enlargement of ventricular system (at age 2y)	Delayed myelination (at age 9m)
Kyphosis/ Pectus	+/+++	+/+++	+/+++	+++/+++	+/++	-/++	+/+

Patient	A(VI$_3$)	A(VI$_4$)	A(VI$_5$)	A(V$_6$)	A(VI$_{10}$)	B(IV$_2$)	A(VI$_1$)
Carinatum							
Hyper-trichosis	+	+	NA	+	+	-	-
Small joints Hyper-flexibility	+	+	++	-	++	+	+
Large joints Contractures	+++ Rocker bottom feet	+++	+++	+++ Rocker bottom feet	+++	++	+
Intensive sweating of palms and feet	+	+	-	+	+	+	+
Miscellaneous	Moderate/ severe hearing impairment SSEP: central bilateral disturbance in central tract conduction above brainstem. Muscle biopsy revealed sediment of	SSEP: central bilateral disturbance in central conduction above brainstem	Muscle biopsy: mild reduction of cytochrome C oxidase activity. Normal Immunohistochemical staining. Normal muscle cells structure .		Occasional horizontal nystagmus. Retinal atrophy with abnormal VEP'S and ERG responses		

Patient	A(VI$_3$)	A(VI$_4$)	A(VI$_5$)	A(V$_6$)	A(VI$_{10}$)	B(IV$_2$)	A(VI$_1$)
	glycogen like material (PAS positive). EM examination confirmed accumulation of glycogen. Normal respiratory chain						

AO, age at onset; FTT, failure to thrive; GMFCS, Gross Motor Functional Classification System; m, months; HC, head circumference

NA, not available.

For all of patients: normal karyotype, level of cholesterol, muscular and lysosomal enzymes

(*) until the age of approximately 5 years followed by an unexplained gradual increase in HC up to 75%.

Figure legends

Figure 1. Pedigree of the investigated families. A. Family I: 6 affected individuals (filled shapes). **B.** Family II: containing another affected individual. A high rate of consanguinity and an AR pattern of inheritance are evident. **C**. Photographs of patient VI_5 (pedigree A) illustrating: coarse facial features (a) pectus carinatum, dystonic posturing, rigidity/freezing and shortening of tendons (b, c), and rocker bottom feet (d).

D. Patients' brain MRI. a and b. T1 Brain MRI of patient IV_2 (family II), at 1 year of age, shows white matter atrophy. Corpus callosum is complete but thin. c (T2 MRI Imaging) and d (T1 MRI Imaging). Brain MRI of patient VI_3 (family I), at 14 years, shows moderate white matter atrophy and severe corpus callosum thinning. e (T2 MRI Imaging) and f (T1 MRI Imaging). Brain MRI of patient V_4 (family I), at age 32 years, shows severe general atrophy. The cortex is usually preserved but very thin, corpus callosum is complete but also very thin. The basal ganglia appear normal.

Figure 2. A. Haplotypes for each family member were constructed for 11 microsatellite markers spanning the neurodegenerative interval. Markers analyzed are given on the left, according to their physical order. Haplotypes are represented by bars, with the disease-associated haplotype shaded in gray. Reduction in the affected linked region to 1.9Mb was due to healthy individuals VI_6 and IV_4 who bear fraction of the affected haplotype in a homozygous manner.

B. Physical location of genes and predicted transcripts in the chromosome 9 linked interval. Asterisk denotes genes not approved by the HUGO Gene Nomenclature Committee (HGNC). “Strand” refers to transcription orientation. Bold names indicate gene analyzed by direct sequencing. Physical location obtained from UCSC Human Genome Browser Gateway (hg19 assembly).**C.** Analysis of the c.2254C>T mutation

in exon 14 of *PLAA*. Sequence analysis is shown for an unaffected individual, an obligatory carrier, and an affected individual. **D.** Sequence alignment of human PLAA to orthologues in the mutation area. The leucine at position 752 (*boxed*) in this protein is highly conserved throughout evolution. **E**. Effect of L752F (Leu→Phe) substitution on PLAA structure. Shown is a ribbon diagram of the PUL domain of PLAA (PDB ID 3EBB) which adopts a banana like shaped Armadillo domain. The conserved residues of PLAA (*homo sapiens*, *mus musculus*, *rattus norvegicus*, *Xenopus laevis*, and *Saccharomyces cerevisiae*) are displayed in stick-representation and form the putative binding site of PLAA. Mutation of Leu752 shown in ball-representation disrupts the rigid leucine network that tightly holds together the Armadillo domain.

Figure 3. mRNA levels for *PLAA* and confocal microscopy of fibroblasts for the presence of PLAA protein. A. Presence of full length transcript for *PLAA* from fibroblasts of affected patients and the control subject based on PCR. **B.** RT-qPCR for the detection of *PLAA* transcript from fibroblasts of a patient versus the healthy control normalized to four house-keeping genes coding for human 18S RNA, GAPDH, PolB, and L19 ribosomal protein. Arithmetic means ± standard deviations from three biological replicates performed in triplicate were shown. **C.** Fibroblasts (n*PLAA* or m*PLAA*) were counterstained with DAPI (blue) for the nucleus and with fluorophore conjugated phalloidin (red) for actin. Cells were fixed, subjected to immunofluorescence staining for PLAA (green), and observed by confocal microscopy. **D.** Mean fluorescence intensity of regions of interest corresponding to the cytoplasm and nucleus of imaged cells (Image J processing program, NIH). Figure represents results from 3 sets of images and error bars represent standard deviations.

Figure 4. PGE_2 levels and $cPLA_2$ activity are low in patients' fibroblasts, and could be rescued. A. Levels of PGE_2 in cell culture media after 24 hours of stimulation with LPS or cholera toxin Levels of PGE_2 were normalized against protein concentrations in the supernatants. All cells were primary human fibroblasts except RAW 264.7 cells which are murine macrophage like cells and used as a positive control. **B.** Activity of $cPLA_2$ in the membrane fractions of fibroblasts and RAW 264.7 macrophages. Cells were stimulated with or without LPS for 24 hours before harvesting and purification of the membrane fractions. The $cPLA_2$ activity was normalized to amount of proteins added to the assay. **C.** PGE_2 levels in the cell culture media after transfection with CMV promoter-based pIRES2-DsRed2 plasmid containing the native *PLAA* gene and a fluorescent marker of transfection. Cells were treated as follow: ctl = no transfection; V = transfection with empty vector; *PLAA* = transfection with plasmid vector containing the wild type *PLAA*. **D.** $cPLA_2$ activity from membrane fractions of fibroblasts after transfection with a plasmid containing the n*PLAA* in a CMV promoter-based vector system and a fluorescent marker of transfection. **E-G.** Fold changes in transcripts for IL-6, IL-8, and MIF based on RT-qPCR. Arithmetic means ± standard deviations from three independent experiments performed in triplicate were plotted and the data were analyzed using one way ANOVA with Tukey *post-hoc* correction.

Figure 5. PGE_2 levels in embryonic mouse tissues. WT, $Plaa^{+/-}$, and $Plaa^{-/-}$ embryos were sacrificed at E18.5 and organs were isolated and prostaglandin levels determined for the lung (**A**), brain (**B**), liver (**C**), and heart (**D**). Data represented arithmetic means ± standard deviations from tissues representing 3 WT, 3 $Plaa^{+/-}$, and 4 $Plaa^{-/-}$ embryos and obtained from three independent littermates. Significance was determined by one

way ANOVA with Tukey *post-hoc* correction. * denotes $p<0.05$ *** denotes $p<0.001$.

Figure 6. Histopathology of embryonic mouse tissues. Lungs **(A)**, brain cerebral cortex **(B),** and skin **(C)** were H&E stained and analyzed in a blinded fashion. Tissues representing 2 WT, 2 *Plaa*$^{+/-}$, and 4 *Plaa*$^{-/-}$ embryos were analyzed. Multiple fields for each tissue were visualized and typical representations are shown with magnifications.

References

Atrouni, S., Daraze, A., Tamraz, J., Cassia, A., Caillaud, C., Megarbane, A., 2003. Leukodystrophy associated with oligodontia in a large inbred family: fortuitous association or new entity? Am J Med Genet A. 118A, 76-81.

Baugh, E.H., Lyskov, S., Weitzner, B.D., Gray, J.J., 2011. Real-time PyMOL visualization for Rosetta and PyRosetta. PLoS One. 6, e21931.

Bazan, N.G., Colangelo, V., Lukiw, W.J., 2002. Prostaglandins and other lipid mediators in Alzheimer's disease. Prostaglandins Other Lipid Mediat. 68-69, 197-210.

Bomont, P., Cavalier, L., Blondeau, F., Ben Hamida, C., Belal, S., Tazir, M., Demir, E., Topaloglu, H., Korinthenberg, R., Tuysuz, B., Landrieu, P., Hentati, F., Koenig, M., 2000. The gene encoding gigaxonin, a new member of the cytoskeletal BTB/kelch repeat family, is mutated in giant axonal neuropathy. Nat Genet. 26, 370-4.

Calignano, A., Piomelli, D., Sacktor, T.C., Schwartz, J.H., 1991. A phospholipase A2-stimulating protein regulated by protein kinase C in Aplysia neurons. Brain Res Mol Brain Res. 9, 347-51.

Cho, J.S., Han, I.H., Lee, H.R., Lee, H.M., 2014. Prostaglandin E2 Induces IL-6 and IL-8 Production by the EP Receptors/Akt/NF-kappaB Pathways in Nasal Polyp-Derived Fibroblasts. Allergy Asthma Immunol Res. 6, 449-57.

Clark, M.A., Ozgur, L.E., Conway, T.M., Dispoto, J., Crooke, S.T., Bomalaski, J.S., 1991. Cloning of a phospholipase A2-activating protein. Proc Natl Acad Sci U S A. 88, 5418-22.

Doroudi, M., Boyan, B.D., Schwartz, Z., 2014. Rapid 1alpha,25(OH)(2)D (3) membrane-mediated activation of Ca(2)(+)/calmodulin-dependent protein kinase II in growth plate chondrocytes requires Pdia3, PLAA and caveolae. Connect Tissue Res. 55 Suppl 1, 125-8.

Feenstra, I., Vissers, L.E., Orsel, M., van Kessel, A.G., Brunner, H.G., Veltman, J.A., van Ravenswaaij-Arts, C.M., 2007. Genotype-phenotype mapping of chromosome 18q deletions by high-resolution array CGH: an update of the phenotypic map. Am J Med Genet A. 143A, 1858-67.

FitzGerald, G.A., 2003. COX-2 and beyond: Approaches to prostaglandin inhibition in human disease. Nat Rev Drug Discov. 2, 879-90.

Gregory, A., Westaway, S.K., Holm, I.E., Kotzbauer, P.T., Hogarth, P., Sonek, S., Coryell, J.C., Nguyen, T.M., Nardocci, N., Zorzi, G., Rodriguez, D., Desguerre, I., Bertini, E., Simonati, A., Levinson, B., Dias, C., Barbot, C., Carrilho, I., Santos, M., Malik, I., Gitschier, J., Hayflick, S.J., 2008. Neurodegeneration associated with genetic defects in phospholipase A(2). Neurology. 71, 1402-9.

Haara, O., Fujimori, S., Schmidt-Ullrich, R., Hartmann, C., Thesleff, I., Mikkola, M.L., 2011. Ectodysplasin and Wnt pathways are required for salivary gland branching morphogenesis. Development. 138, 2681-91.

Han, C., Lim, K., Xu, L., Li, G., Wu, T., 2008. Regulation of Wnt/beta-catenin pathway by cPLA2alpha and PPARdelta. J Cell Biochem. 105, 534-45.

Hatzfeld, M., 1999. The armadillo family of structural proteins. Int Rev Cytol. 186, 179-224.

Henneke, M., Combes, P., Diekmann, S., Bertini, E., Brockmann, K., Burlina, A.P., Kaiser, J., Ohlenbusch, A., Plecko, B., Rodriguez, D., Boespflug-Tanguy, O.,

Gartner, J., 2008. GJA12 mutations are a rare cause of Pelizaeus-Merzbacher-like disease. Neurology. 70, 748-54.

Henneke, M., Diekmann, S., Ohlenbusch, A., Kaiser, J., Engelbrecht, V., Kohlschutter, A., Kratzner, R., Madruga-Garrido, M., Mayer, M., Opitz, L., Rodriguez, D., Ruschendorf, F., Schumacher, J., Thiele, H., Thoms, S., Steinfeld, R., Nurnberg, P., Gartner, J., 2009. RNASET2-deficient cystic leukoencephalopathy resembles congenital cytomegalovirus brain infection. Nat Genet. 41, 773-5.

Jin, D., Ni, T.T., Sun, J., Wan, H., Amack, J.D., Yu, G., Fleming, J., Chiang, C., Li, W., Papierniak, A., Cheepala, S., Conseil, G., Cole, S.P., Zhou, B., Drummond, I.A., Schuetz, J.D., Malicki, J., Zhong, T.P., 2014. Prostaglandin signalling regulates ciliogenesis by modulating intraflagellar transport. Nat Cell Biol. 16, 841-51.

Joksimovic, M., Awatramani, R., 2014. Wnt/beta-catenin signaling in midbrain dopaminergic neuron specification and neurogenesis. J Mol Cell Biol. 6, 27-33.

Khateeb, S., Flusser, H., Ofir, R., Shelef, I., Narkis, G., Vardi, G., Shorer, Z., Levy, R., Galil, A., Elbedour, K., Birk, O.S., 2006. PLA2G6 mutation underlies infantile neuroaxonal dystrophy. Am J Hum Genet. 79, 942-8.

Lamari, F., Mochel, F., Sedel, F., Saudubray, J.M., 2013. Disorders of phospholipids, sphingolipids and fatty acids biosynthesis: toward a new category of inherited metabolic diseases. J Inherit Metab Dis. 36, 411-25.

Lee, L.Y., Farooqui, A.A., Dawe, G.S., Burgunder, J.M., Ong, W.Y., 2009. Role of phospholipase A(2) in prepulse inhibition of the auditory startle reflex in rats. Neurosci Lett. 453, 6-8.

Li, X., Okada, Y., Pilbeam, C.C., Lorenzo, J.A., Kennedy, C.R., Breyer, R.M., Raisz, L.G., 2000. Knockout of the murine prostaglandin EP2 receptor impairs osteoclastogenesis in vitro. Endocrinology. 141, 2054-61.

Loureiro, J., Peifer, M., 1998. Roles of Armadillo, a Drosophila catenin, during central nervous system development. Curr Biol. 8, 622-32.

Magen, D., Georgopoulos, C., Bross, P., Ang, D., Segev, Y., Goldsher, D., Nemirovski, A., Shahar, E., Ravid, S., Luder, A., Heno, B., Gershoni-Baruch, R., Skorecki, K., Mandel, H., 2008. Mitochondrial hsp60 chaperonopathy causes an autosomal-recessive neurodegenerative disorder linked to brain hypomyelination and leukodystrophy. Am J Hum Genet. 83, 30-42.

Mertin, J., Stackpoole, A., 1978. Suppression by essential fatty acids of experimental allergic encephalomyelitis is abolished by indomethacin. Prostaglandins Med. 1, 283-91.

Milatovic, D., Montine, T.J., Aschner, M., 2011. Prostanoid signaling: dual role for prostaglandin E2 in neurotoxicity. Neurotoxicology. 32, 312-9.

Mohri, I., Taniike, M., Taniguchi, H., Kanekiyo, T., Aritake, K., Inui, T., Fukumoto, N., Eguchi, N., Kushi, A., Sasai, H., Kanaoka, Y., Ozono, K., Narumiya, S., Suzuki, K., Urade, Y., 2006. Prostaglandin D2-mediated microglia/astrocyte interaction enhances astrogliosis and demyelination in twitcher. J Neurosci. 26, 4383-93.

Mullally, J.E., Chernova, T., Wilkinson, K.D., 2006. Doa1 is a Cdc48 adapter that possesses a novel ubiquitin binding domain. Mol Cell Biol. 26, 822-30.

Nakatani, Y., Hokonohara, Y., Kakuta, S., Sudo, K., Iwakura, Y., Kudo, I., 2007. Knockout mice lacking cPGES/p23, a constitutively expressed PGE2 synthetic enzyme, are peri-natally lethal. Biochem Biophys Res Commun. 362, 387-92.

Nguyen, M., Camenisch, T., Snouwaert, J.N., Hicks, E., Coffman, T.M., Anderson, P.A., Malouf, N.N., Koller, B.H., 1997. The prostaglandin receptor EP4 triggers remodelling of the cardiovascular system at birth. Nature. 390, 78-81.

Nissim, S., Sherwood, R.I., Wucherpfennig, J., Saunders, D., Harris, J.M., Esain, V., Carroll, K.J., Frechette, G.M., Kim, A.J., Hwang, K.L., Cutting, C.C., Elledge, S., North, T.E., Goessling, W., 2014. Prostaglandin E2 regulates liver versus pancreas cell-fate decisions and endodermal outgrowth. Dev Cell. 28, 423-37.

Palisano, R., Rosenbaum, P., Walter, S., Russell, D., Wood, E., Galuppi, B., 1997. Development and reliability of a system to classify gross motor function in children with cerebral palsy. Dev Med Child Neurol. 39, 214-23.

Palumbo, S., Toscano, C.D., Parente, L., Weigert, R., Bosetti, F., 2011. Time-dependent changes in the brain arachidonic acid cascade during cuprizone-induced demyelination and remyelination. Prostaglandins Leukot Essent Fatty Acids. 85, 29-35.

Pusch, C., Hustert, E., Pfeifer, D., Sudbeck, P., Kist, R., Roe, B., Wang, Z., Balling, R., Blin, N., Scherer, G., 1998. The SOX10/Sox10 gene from human and mouse: sequence, expression, and transactivation by the encoded HMG domain transcription factor. Hum Genet. 103, 115-23.

Qiu, L., Pashkova, N., Walker, J.R., Winistorfer, S., Allali-Hassani, A., Akutsu, M., Piper, R., Dhe-Paganon, S., 2010. Structure and function of the PLAA/Ufd3-p97/Cdc48 complex. J Biol Chem. 285, 365-72.

Ribardo, D.A., Peterson, J.W., Chopra, A.K., 2002. Phospholipase A2-activating protein--an important regulatory molecule in modulating cyclooxygenase-2 and tumor necrosis factor production during inflammation. Indian J Exp Biol. 40, 129-38.

Ruprecht, K., Warmuth-Metz, M., Waespe, W., Gold, R., 2002. Symptomatic hyperekplexia in a patient with multiple sclerosis. Neurology. 58, 503-4.

Schmitz, M., Hermann, P., Oikonomou, P., Stoeck, K., Ebert, E., Poliakova, T., Schmidt, C., Llorens, F., Zafar, S., Zerr, I., 2015. Cytokine profiles and the role of cellular prion protein in patients with vascular dementia and vascular encephalopathy. Neurobiol Aging. 36, 2597-606.

Sievers, F., Wilm, A., Dineen, D., Gibson, T.J., Karplus, K., Li, W., Lopez, R., McWilliam, H., Remmert, M., Soding, J., Thompson, J.D., Higgins, D.G., 2011. Fast, scalable generation of high-quality protein multiple sequence alignments using Clustal Omega. Mol Syst Biol. 7, 539.

Tazir, M., Nouioua, S., Magy, L., Huehne, K., Assami, S., Urtizberea, A., Grid, D., Hamadouche, T., Rautenstrauss, B., Vallat, J.M., 2009. Phenotypic variability in giant axonal neuropathy. Neuromuscul Disord. 19, 270-4.

Teer, J.K., Bonnycastle, L.L., Chines, P.S., Hansen, N.F., Aoyama, N., Swift, A.J., Abaan, H.O., Albert, T.J., Margulies, E.H., Green, E.D., Collins, F.S., Mullikin, J.C., Biesecker, L.G., 2010. Systematic comparison of three genomic enrichment methods for massively parallel DNA sequencing. Genome Res. 20, 1420-31.

Teer, J.K., Green, E.D., Mullikin, J.C., Biesecker, L.G., 2012. VarSifter: visualizing and analyzing exome-scale sequence variation data on a desktop computer. Bioinformatics. 28, 599-600.

Timmons, M., Tsokos, M., Asab, M.A., Seminara, S.B., Zirzow, G.C., Kaneski, C.R., Heiss, J.D., van der Knaap, M.S., Vanier, M.T., Schiffmann, R., Wong, K., 2006. Peripheral and central hypomyelination with hypogonadotropic hypogonadism and hypodontia. Neurology. 67, 2066-9.

Toribio, R.E., Brown, H.A., Novince, C.M., Marlow, B., Hernon, K., Lanigan, L.G., Hildreth, B.E., 3rd, Werbeck, J.L., Shu, S.T., Lorch, G., Carlton, M., Foley, J., Boyaka, P., McCauley, L.K., Rosol, T.J., 2010. The midregion, nuclear localization sequence, and C terminus of PTHrP regulate skeletal development, hematopoiesis, and survival in mice. FASEB J. 24, 1947-57.

Uhlenberg, B., Schuelke, M., Ruschendorf, F., Ruf, N., Kaindl, A.M., Henneke, M., Thiele, H., Stoltenburg-Didinger, G., Aksu, F., Topaloglu, H., Nurnberg, P., Hubner, C., Weschke, B., Gartner, J., 2004. Mutations in the gene encoding gap junction protein alpha 12 (connexin 46.6) cause Pelizaeus-Merzbacher-like disease. Am J Hum Genet. 75, 251-60.

van der Knaap, M.S., Barth, P.G., Stroink, H., van Nieuwenhuizen, O., Arts, W.F., Hoogenraad, F., Valk, J., 1995. Leukoencephalopathy with swelling and a discrepantly mild clinical course in eight children. Ann Neurol. 37, 324-34.

van der Knaap, M.S., 2001. Magnetic resonance in childhood white-matter disorders. Dev Med Child Neurol. 43, 705-12.

Weidenheim, K.M., Dickson, D.W., Rapin, I., 2009. Neuropathology of Cockayne syndrome: Evidence for impaired development, premature aging, and neurodegeneration. Mech Ageing Dev. 130, 619-36.

Yu, Y., Fan, J., Chen, X.S., Wang, D., Klein-Szanto, A.J., Campbell, R.L., FitzGerald, G.A., Funk, C.D., 2006. Genetic model of selective COX2 inhibition reveals novel heterodimer signaling. Nat Med. 12, 699-704.

Zhang, F., Sha, J., Wood, T.G., Galindo, C.L., Garner, H.R., Burkart, M.F., Suarez, G., Sierra, J.C., Agar, S.L., Peterson, J.W., Chopra, A.K., 2008. Alteration in the activation state of new inflammation-associated targets by phospholipase A2-activating protein (PLAA). Cell Signal. 20, 844-61.

Zhang, S., Li, J., Lea, R., Vleminckx, K., Amaya, E., 2014. Fezf2 promotes neuronal differentiation through localised activation of Wnt/beta-catenin signalling during forebrain development. Development. 141, 4794-805.

Zivony-Elboum, Y., Westbroek, W., Kfir, N., Savitzki, D., Shoval, Y., Bloom, A., Rod, R., Khayat, M., Gross, B., Samri, W., Cohen, H., Sonkin, V., Freidman, T., Geiger, D., Fattal-Valevski, A., Anikster, Y., Waters, A.M., Kleta, R., Falik-Zaccai, T.C., 2012. A founder mutation in Vps37A causes autosomal recessive complex hereditary spastic paraparesis. J Med Genet. 49, 462-72.

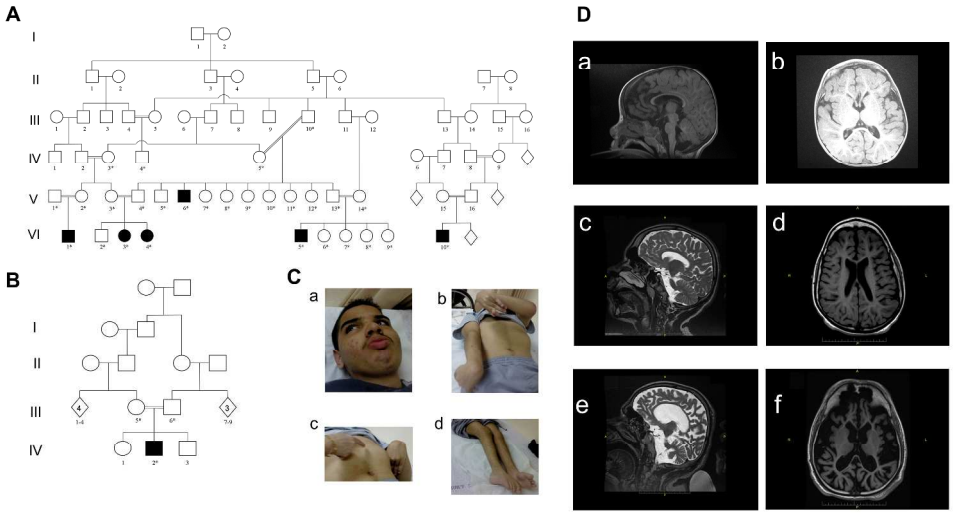

Figure 1. Pedigree of the investigated families. A. Family I: 6 affected individuals (filled shapes). B. Family II: containing another affected individual. A high rate of consanguinity and an AR pattern of inheritance are evident. C. Photographs of patient VI5 (pedigree A) illustrating: coarse facial features (a) pectus carinatum, dystonic posturing, rigidity/freezing and shortening of tendons (b, c), and rocker bottom feet (d).
D. Patients' brain MRI. a and b. T1 Brain MRI of patient IV2 (family II), at 1 year of age, shows white matter atrophy. Corpus callosum is complete but thin. c (T2 MRI Imaging) and d (T1 MRI Imaging). Brain MRI of patient VI3 (family I), at 14 years, shows moderate white matter atrophy and severe corpus callosum thinning. e (T2 MRI Imaging) and f (T1 MRI Imaging). Brain MRI of patient V4 (family I), at age 32 years, shows severe general atrophy. The cortex is usually preserved but very thin, corpus callosum is complete but also very thin. The basal ganglia appear normal.

338x190mm (300 x 300 DPI)

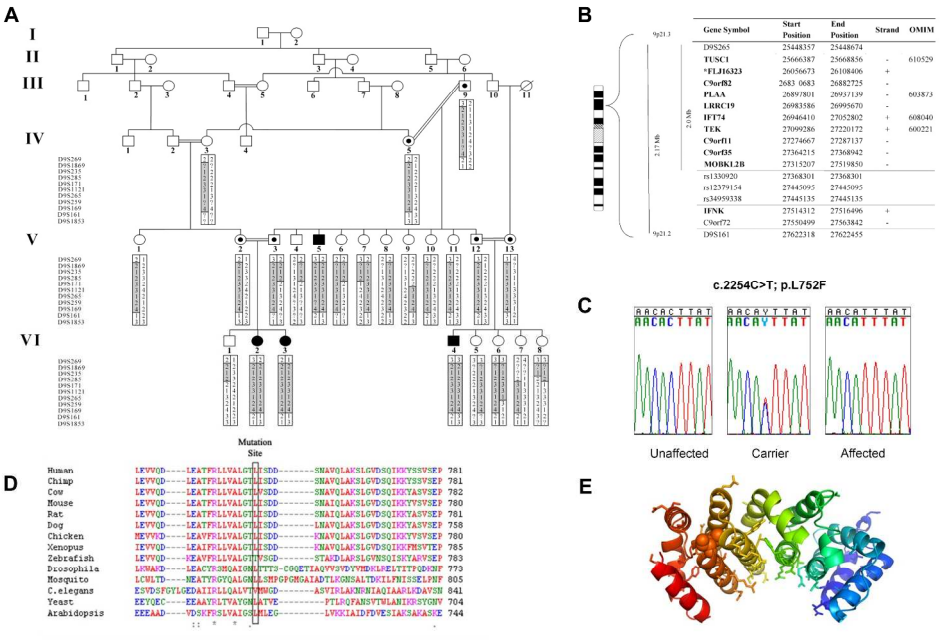

Figure 2. A. Haplotypes for each family member were constructed for 11 microsatellite markers spanning the neurodegenerative interval. Markers analyzed are given on the left, according to their physical order. Haplotypes are represented by bars, with the disease-associated haplotype shaded in gray. Reduction in the affected linked region to 1.9Mb was due to healthy individuals VI6 and IV4 who bear fraction of the affected haplotype in a homozygous manner.

B. Physical location of genes and predicted transcripts in the chromosome 9 linked interval. Asterisk denotes genes not approved by the HUGO Gene Nomenclature Committee (HGNC). "Strand" refers to transcription orientation. Bold names indicate gene analyzed by direct sequencing. Physical location obtained from UCSC Human Genome Browser Gateway (hg19 assembly).C. Analysis of the c.2254C>T mutation in exon 14 of PLAA. Sequence analysis is shown for an unaffected individual, an obligatory carrier, and an affected individual. D. Sequence alignment of human PLAA to orthologues in the mutation area. The leucine at position 752 (boxed) in this protein is highly conserved throughout evolution. E. Effect of L752F (Leu→Phe) substitution on PLAA structure. Shown is a ribbon diagram of the PUL domain of PLAA (PDB ID 3EBB) which adopts a banana like shaped Armadillo domain. The conserved residues of PLAA (homo sapiens, mus musculus, rattus norvegicus, Xenopus laevis, and Saccharomyces cerevisiae) are displayed in stick-representation and form the putative binding site of PLAA. Mutation of Leu752 shown in ball-representation disrupts the rigid leucine network that tightly holds together the Armadillo domain.

457x304mm (300 x 300 DPI)

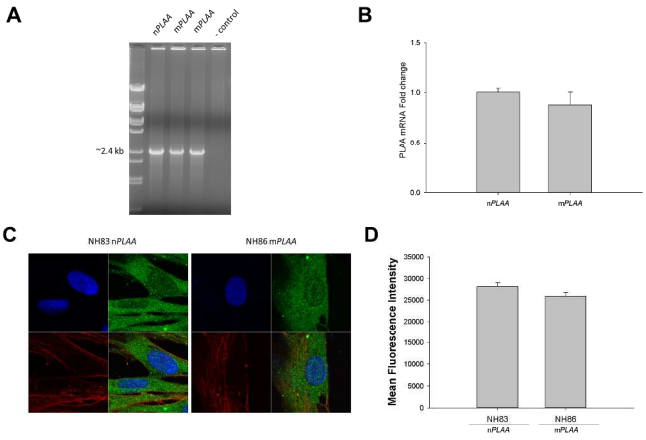

Figure 3. mRNA levels for PLAA and confocal microscopy of fibroblasts for the presence of PLAA protein. A. Presence of full length transcript for PLAA from fibroblasts of affected patients and the control subject based on PCR. B. RT-qPCR for the detection of PLAA transcript from fibroblasts of a patient versus the healthy control normalized to four house-keeping genes coding for human 18S RNA, GAPDH, PolB, and L19 ribosomal protein. Arithmetic means ± standard deviations from three biological replicates performed in triplicate were shown. C. Fibroblasts (nPLAA or mPLAA) were counterstained with DAPI (blue) for the nucleus and with fluorophore conjugated phalloidin (red) for actin. Cells were fixed, subjected to immunofluorescence staining for PLAA (green), and observed by confocal microscopy. D. Mean fluorescence intensity of regions of interest corresponding to the cytoplasm and nucleus of imaged cells (Image J processing program, NIH). Figure represents results from 3 sets of images and error bars represent standard deviations.

338x190mm (300 x 300 DPI)

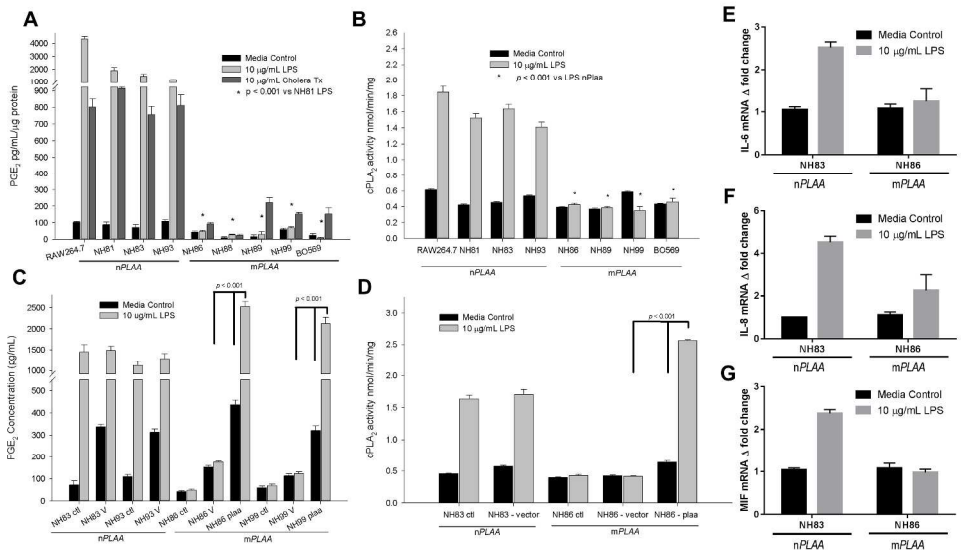

Figure 4. PGE2 levels and cPLA2 activity are low in patients' fibroblasts, and could be rescued. A. Levels of PGE2 in cell culture media after 24 hours of stimulation with LPS or cholera toxin Levels of PGE2 were normalized against protein concentrations in the supernatants. All cells were primary human fibroblasts except RAW 264.7 cells which are murine macrophage like cells and used as a positive control. B. Activity of cPLA2 in the membrane fractions of fibroblasts and RAW 264.7 macrophages. Cells were stimulated with or without LPS for 24 hours before harvesting and purification of the membrane fractions. The cPLA2 activity was normalized to amount of proteins added to the assay. C. PGE2 levels in the cell culture media after transfection with CMV promoter-based pIRES2-DsRed2 plasmid containing the native PLAA gene and a fluorescent marker of transfection. Cells were treated as follow: ctl = no transfection; V = transfection with empty vector; PLAA = transfection with plasmid vector containing the wild type PLAA. D. cPLA2 activity from membrane fractions of fibroblasts after transfection with a plasmid containing the nPLAA in a CMV promoter-based vector system and a fluorescent marker of transfection. E-G. Fold changes in transcripts for IL-6, IL-8, and MIF based on RT-qPCR. Arithmetic means ± standard deviations from three independent experiments performed in triplicate were plotted and the data were analyzed using one way ANOVA with Tukey post-hoc correction.

338x190mm (300 x 300 DPI)

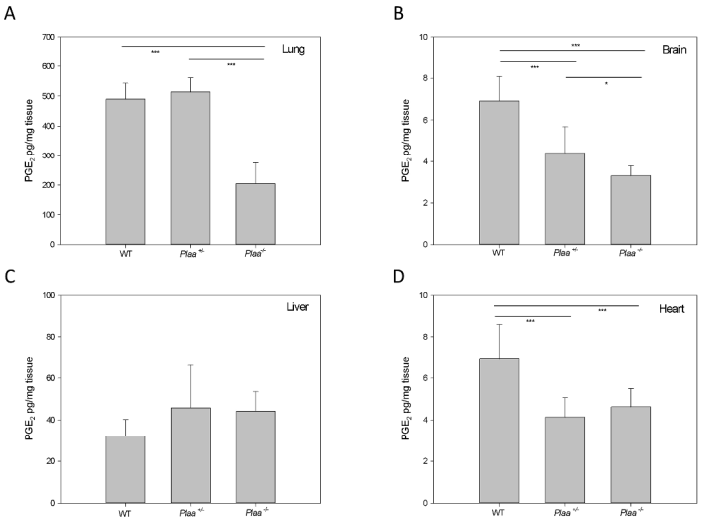

Figure 5. PGE2 levels in embryonic mouse tissues. WT, Plaa+/-, and Plaa-/- embryos were sacrificed at E18.5 and organs were isolated and prostaglandin levels determined for the lung (A), brain (B), liver (C), and heart (D). Data represented arithmetic means ± standard deviations from tissues representing 3 WT, 3 Plaa+/-, and 4 Plaa-/- embryos and obtained from three independent littermates. Significance was determined by one way ANOVA with Tukey post-hoc correction. * denotes $p<0.05$ *** denotes $p<0.001$.

338x190mm (300 x 300 DPI)

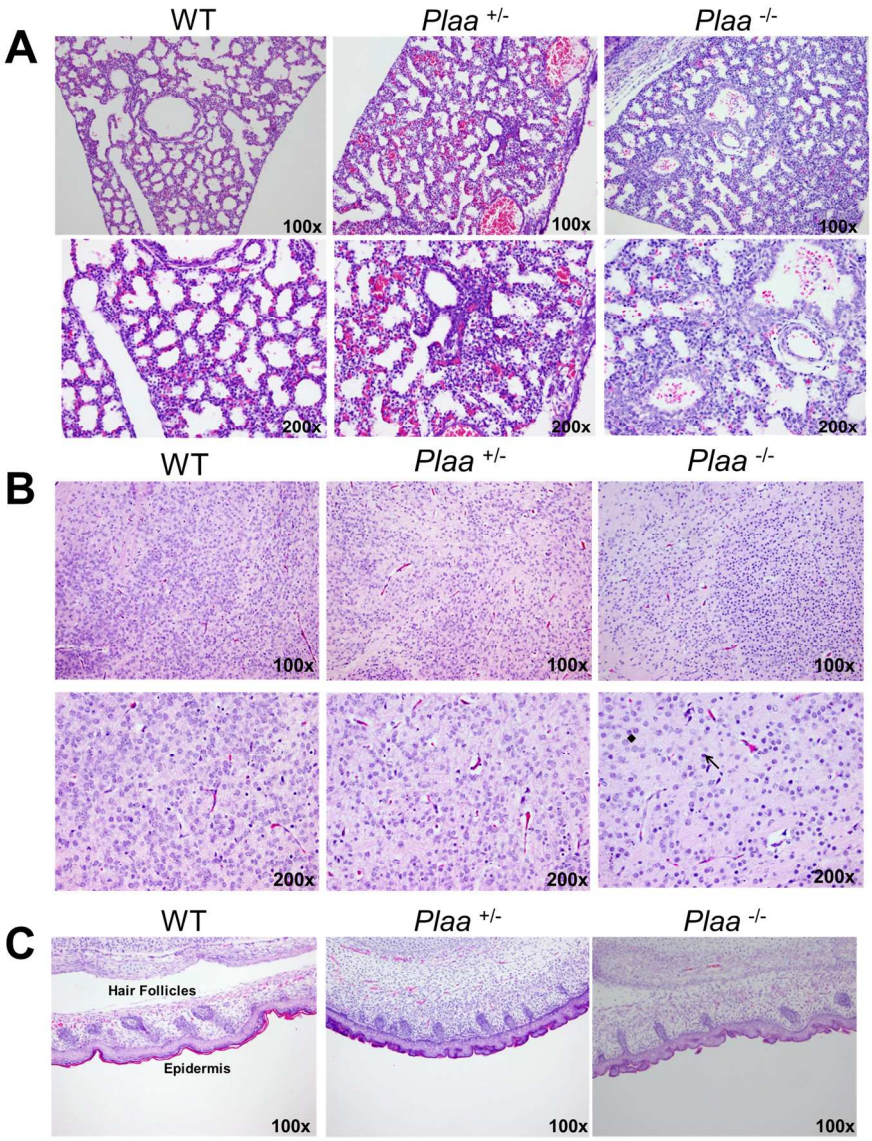

Figure 6. Histopathology of embryonic mouse tissues. Lungs (A), brain cerebral cortex (B), and skin (C) were H&E stained and analyzed in a blinded fashion. Tissues representing 2 WT, 2 Plaa+/-, and 4 Plaa-/- embryos were analyzed. Multiple fields for each tissue were visualized and typical representations are shown with magnifications.

152x190mm (300 x 300 DPI)

Supplementary Materials and Methods

Western blot analysis

Ubiquitin. Western blotting was performed with a SDS-PAGE Electrophoresis System as described previously (Khayat *et al.*, 2008). Briefly, 30 µg protein samples from healthy controls' and patients' fibroblasts were prepared in a reducing sample buffer, and then electrophoresed on a 7.5% Tris gel with Tris running buffer; blotted to nitrocellulose membrane; and probed with mouse anti-ubiquitin (Santa Cruz Biotechnology, Inc., Santa Cruz, CA) antibodies. A horseradish peroxidase-conjugated goat anti-mouse secondary antibody (Santa Cruz) was then added, and proteins detected by autoradiography using enhanced chemiluminescence substrate (Pierce ECL kit, Thermo Scientific, Grand Island, NY).

Yeast experiments

Wild type *DOA1* gene expressing plasmid and *DOA1* deleted yeast strain (*Saccharomyces cerevisiae*) were kindly provided by Prof. Tzachi Pilpel and Dr. Orna Dahan (Weizmann Institute of Science, Israel). Mutant p.Leu677Phe (Leucine→ Phenylalanine) *DOA1* was produced using the Quikchange site-directed Wild type or mutant *DOA1* expressing plasmid, or a mock plasmid, was transformed into the indicated yeast strain by standard lithium acetate method. The yeast was grown on a regular synthetic medium at 30^{o}C, 37^{o}C or at 30^{o}C supplemented with 0.5 µg/ml cycloheximide. After three days, the growth of the yeast was assessed.

Cell biology studies

Immunofluorescence Confocal Microscopy

Confocal microscopy was performed on fixed fibroblasts by established procedures with slight modifications. Briefly, nPLAA and mPLAA were treated with 10 µg/mL LPS for 60 min, with LPS untreated cells serving as controls, before fixation with 4% paraformaldehyde. Subsequently, fibroblasts were permeabilized with 0.5% Triton X-100. Goat anti-p65 C-20 antibody (Santa Cruz) or rabbit anti-PLAA antibody (GenWay Biotech, Inc., San Diego, CA), and Alexa Fluor 488 donkey anti-goat antibody (Molecular Probes, Carlsbad, CA) or Alexa Fluor 488 donkey anti-rabbit antibody, were used as primary and secondary antibodies, respectively, as appropriate. Samples stained with secondary antibody alone were used as negative controls. Fibroblasts were then counterstained with DAPI (Life Technologies, Grand Island, NY) and Alexa Fluor 594 phalloidin (Life Technologies) to stain the nucleus and actin, respectively. Fibroblasts were subsequently visualized using a Zeiss LSM510 confocal scanning microscope.

Plaa Gene Targeting

A mouse genomic library, ES129SvJ, was screened for clones containing the *Plaa* gene. Two overlapping pUC18 clones, 10-1-1A carrying a ~17-kb *Plaa* upstream-intron 2 region and 7-2-1A carrying a ~12-kb *Plaa* intron 2-intron 10 region, were validated for the organization of the gene by DNA restriction enzyme digestion and sequence analysis, and used for knockout vector construction. A 3.1-kb *Hin*dIII-*Bgl*II fragment (intron 1, 5' homology arm), and a 6.0-kb *Sal*I-*Asp*718 (located in pUC18) fragment containing exons 8-10 (3' homology arm) were subcloned into a plasmid vector, pBluescript II KS (-) (Agilent Technologies). A positive selection marker PGK*neobpA* (Soriano *et al.*, 1991) flanked by *loxP* sites was inserted between two homology arms, and a negative selection marker HSV*tkpA* (Mansour *et al.,* 1988) was inserted between pBluescript and the 5' homology arm (**Figure S2, A**).

The vector was linearized at the end of the 3' homology arm by *Asp*718 and electroporated into 129S inbred Tc1 (George et al., 2007)kindly provided by Phillip Leder, Harvard Medical School, Boston, MA) and B6129F$_1$ hybrid G4 (George et al., 2007) kindly provided by Andras Nagy, Samuel Lunenfeld Research Institute, Mount Sinai Hospital, NY) mouse embryonic stem (ES) cells.

A 3'-flanking probe was used in Southern blot for the identification of targeted clones (**Figure S2, A**). Mutant ES cell clones were injected into C57BL/6J blastocysts. We crossed chimeric mice and C57BL/6J to produce animals heterozygous for the *Plaa* knockout (KO)^{neo} allele. To establish mutant lines with *Plaa* exon-2-7 deletion (KO) allele, we crossed KO^{neo}/+ mice to a germ-line *cre* deleter strain, Zp3-cre transgenic mouse, on a C57BL/6J background (Lewandoski et al., 1997)C57BL/6J-Tg(Zp3-*cre*)93Knw/J, The Jackson Laboratory, Stock Number: 003651). The mice were maintained by backcrossing to C57BL/6J.

Genotyping

We genotyped mice initially by Southern blot analysis using the 3' probe, and subsequently by PCR (**Figure S2, B&C**). The 3' probe was generated by PCR with primers: XB-X-*Plaa*, 5'-CTTCTCGAGTTCCTGAATGTCTGGGAAAA-3'; and XB-B-*Plaa*, 5'-ACGAGATCTAGTGATGTGGCAATGCCTTT-3'; and mouse genomic DNA as the template. The PCR product was treated with Klenow DNA polymerase, digested with *Bgl*II, and subcloned into pBluescript II SK (-) at *Eco*RV and *Bam*HI sites (p*Plaa* 3' XB). The digestion of the plasmid p*Plaa* 3' XB by *Xho*I and *Xba*I restriction enzymes released a ~450-bp DNA fragment corresponding to *Plaa* exon 13 and its flanking region. Genotyping PCR was performed with the following primers: PlaaWTF, 5'-GGGGGTGGCGTTCCATGTGT-3'; PlaaM+F, 5'-GTGGGGCAGGACAGCAAG-3'; PlaaM-F, 5'-CCATTTGGCTTTTTGGTCTT-3';

and PlaaCMR, 5'-CCACCTCCCGTCACTAACACTCCA-3'. PCR conditions for the genotyping will be provided upon request.

Supplementary Results

Functional Effects of p.Leu752Phe on PLAA

While the Δ*DOA1* strain displayed abrogated growth, transformation of the Δ*DOA1* strain with a plasmid expressing either the native *DOA1* gene or its p.Leu677Phe variant, which corresponds to Leu752 in human PLAA, completely rescued the growth phenotype of *S. cerevisiae* Δ*DOA1* mutant strain (data not shown). Likewise, we found no evidence of effect of p.Leu752Phe variation of PLAA on ubiquitin depletion in fibroblasts from healthy controls versus patients based on Western blot analysis (data not shown).

NF-κB Recruitment to the Nucleus is Unaffected by p.Leu752Phe in the PLAA.

As the secretion of PGE_2 as well as the activity of $cPLA_2$ was decreased in m*PLAA* fibroblasts, we investigated whether NF-κB signaling was intact. We stimulated n*PLAA* and m*PLAA* cells with 10 μg/mL LPS for 60 min and compared nuclear localization of p65 by confocal microscopy. Unstimulated n*PLAA* and m*PLAA* fibroblasts exhibited comparable fluorescent staining primarily in the cytoplasm with little to no nuclear staining (**Figure S1**A,B). Upon stimulation with LPS, both n*PLAA* and m*PLAA* fibroblasts showed localized NF-κB staining primarily in the nucleus, with no significant differences between cell types (n*PLAA* versus m*PLAA* fibroblasts). These data suggested that the NF-κB signaling pathway remained intact and that differences in phenotype observed for m*PLAA* fibroblasts could be localized downstream of NF-κB signaling.

Wnt Signaling is Not Affected by p.Leu752Phe PLAA

β-catenin mediated wingless integration (Wnt) signaling has been shown to play an important role in early embryonic development, neurogenesis, central nervous system morphogenesis, hirsutism, sweat gland morphology, short tendons, and kyphosis (Haara et al., 2011 ; Joksimovic and Awatramani, 2014; Toribio et al., 2010; Zhang et al., 2014).(Chenn, 2008). Han and collegues have shown this pathway to be regulated by cPLA2a (Han et al., 2008). Therefore, we investigated Wnt signaling by examining levels of non-phospho (active) β-catenin in n*PLAA* versus m*PLAA* fibroblasts with and without LPS stimulation. As shown in **Figure S1C**, the levels of active β-catenin were increased after LPS stimulation to a similar extent in both types of fibroblasts. These data indicated that the variant *PLAA* in our patients did not alter canonical Wnt signaling pathway.

Supplementary Figure Legends

Figure S1. Evaluation of NF-κB translocation and Wnt signaling. **A.** Samples (see legends for Figure 4) were counterstained with DAPI (blue) for the nucleus and with fluorophore conjugated phalloidin (red) for actin. Cells were stimulated with or without LPS for 1 h, then fixed and subjected to immunofluorescence staining for p65 of NF-κB (green). **B.** Mean fluorescence intensity of regions of interest (Image J processing program) corresponding to the nucleus and cytoplasm of cells stimulated with and without LPS is shown. Figure represents results from 3 sets of images and error bars indicate standard deviations. **C.** The whole cell lysates from n*PLAA* and m*PLAA* fibroblasts with and without LPS treatment were subjected to Western blot analysis and probed with non-phospho (active) β-catenin antibodies. Antibodies to β-tubulin were used as a loading control. Three independent experiments were performed and fold changes in the level of β-catenin (based on densitometer scanning of the bands) and normalized to the internal control with and without LPS treatment are shown.

Figure S2. *Plaa* gene targeting. We replaced an exon-2-7 region of the mouse *Plaa* gene with a *neo* cassette flanked by *loxP* sites. The cassette was subsequently removed *via cre-loxP* recombination. The *Plaa* mutant allele with *neo* cassette and the one without the cassette resulted in the same phenotype. **A.** Maps of the *Plaa* wild-type (WT) allele, knockout (KO) vector, KO^{neo} allele, and KO allele. Exons 1-14 are shown as boxes. Blue, pink, yellow, and red triangles indicate genotyping primers: PlaaWT, PlaaM+F, PlaaM-F, and PlaaCMR, respectively. A, *Asp*718; BI, *Bgl*I; BII, *Bgl*II; H, *Hin*dIII; and S, *Sal*I. **B.** Southern blot analysis of genomic DNA isolated from three *Plaa*-KO^{neo}/+ mouse embryonic stem cell clones and a random integration clone (R). The 3' flanking probe hybridized to a 22.6-kb *Bgl*I DNA fragment from

WT allele, and a 14.7-kb *Bgl*I DNA fragment from KO^{neo} allele. The *neo* probe also hybridized to the 14.7-kb *Bgl*I DNA fragment. We identified three ES cell clones that incoorporated the *Plaa* mutation by Southern blot analysis. The clones #27 and 75 were derived from Tc1 ES cells; the clone #52 was derived from G4 ES cells. The clones #27 and 52 transmitted the mutant allele to the germ line of the mouse. **C.** PCR genotyping of the mouse. The upper panel shows genotyping results for E14.5 embryos produced by *Plaa*-KO^{neo} heterozygous intercrosses; the lower panel shows genotyping results for *Plaa*-KO lines.

References

Chenn, A., 2008. Wnt/beta-catenin signaling in cerebral cortical development. Organogenesis. 4**,** 76-80.

George, S.H., Gertsenstein, M., Vintersten, K., Korets-Smith, E., Murphy, J., Stevens, M.E., Haigh, J.J., Nagy, A., 2007. Developmental and adult phenotyping directly from mutant embryonic stem cells. Proc Natl Acad Sci U S A. 104**,** 4455-60.

Haara, O., Fujimori, S., Schmidt-Ullrich, R., Hartmann, C., Thesleff, I., Mikkola, M.L., 2011. Ectodysplasin and Wnt pathways are required for salivary gland branching morphogenesis. Development. 138**,** 2681-91.

Han, C., Lim, K., Xu, L., Li, G., Wu, T., 2008. Regulation of Wnt/beta-catenin pathway by cPLA2alpha and PPARdelta. J Cell Biochem. 105**,** 534-45.

Joksimovic, M., Awatramani, R., 2014. Wnt/beta-catenin signaling in midbrain dopaminergic neuron specification and neurogenesis. J Mol Cell Biol. 6**,** 27-33.

Khayat, M., Korman, S.H., Frankel, P., Weintraub, Z., Hershckowitz, S., Sheffer, V.F., Ben Elisha, M., Wevers, R.A., Falik-Zaccai, T.C., 2008. PNPO deficiency: an under diagnosed inborn error of pyridoxine metabolism. Mol Genet Metab. 94**,** 431-4.

Lewandoski, M., Wassarman, K.M., Martin, G.R., 1997. Zp3-cre, a transgenic mouse line for the activation or inactivation of loxP-flanked target genes specifically in the female germ line. Curr Biol. 7**,** 148-51.

Mansour, S.L., Thomas, K.R., Capecchi, M.R., 1988. Disruption of the proto-oncogene int-2 in mouse embryo-derived stem cells: a general strategy for targeting mutations to non-selectable genes. Nature. 336**,** 348-52.

Soriano, P., Montgomery, C., Geske, R., Bradley, A., 1991. Targeted disruption of the c-src proto-oncogene leads to osteopetrosis in mice. Cell. 64**,** 693-702.

Toribio, R.E., Brown, H.A., Novince, C.M., Marlow, B., Hernon, K., Lanigan, L.G., Hildreth, B.E., 3rd, Werbeck, J.L., Shu, S.T., Lorch, G., Carlton, M., Foley, J., Boyaka, P., McCauley, L.K., Rosol, T.J., 2010. The midregion, nuclear localization sequence, and C terminus of PTHrP regulate skeletal development, hematopoiesis, and survival in mice. FASEB J. 24**,** 1947-57.

Zhang, S., Li, J., Lea, R., Vleminckx, K., Amaya, E., 2014. Fezf2 promotes neuronal differentiation through localised activation of Wnt/beta-catenin signalling during forebrain development. Development. 141**,** 4794-805.

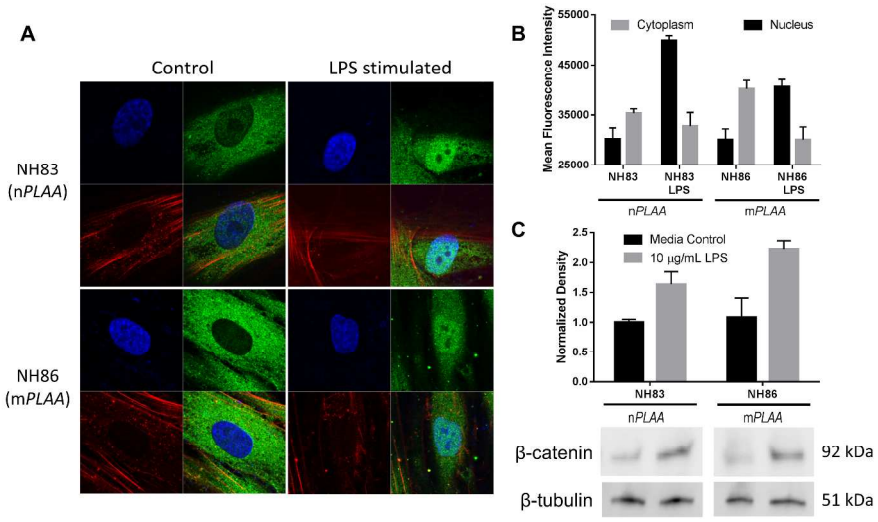

338x190mm (300 x 300 DPI)

Figure S2

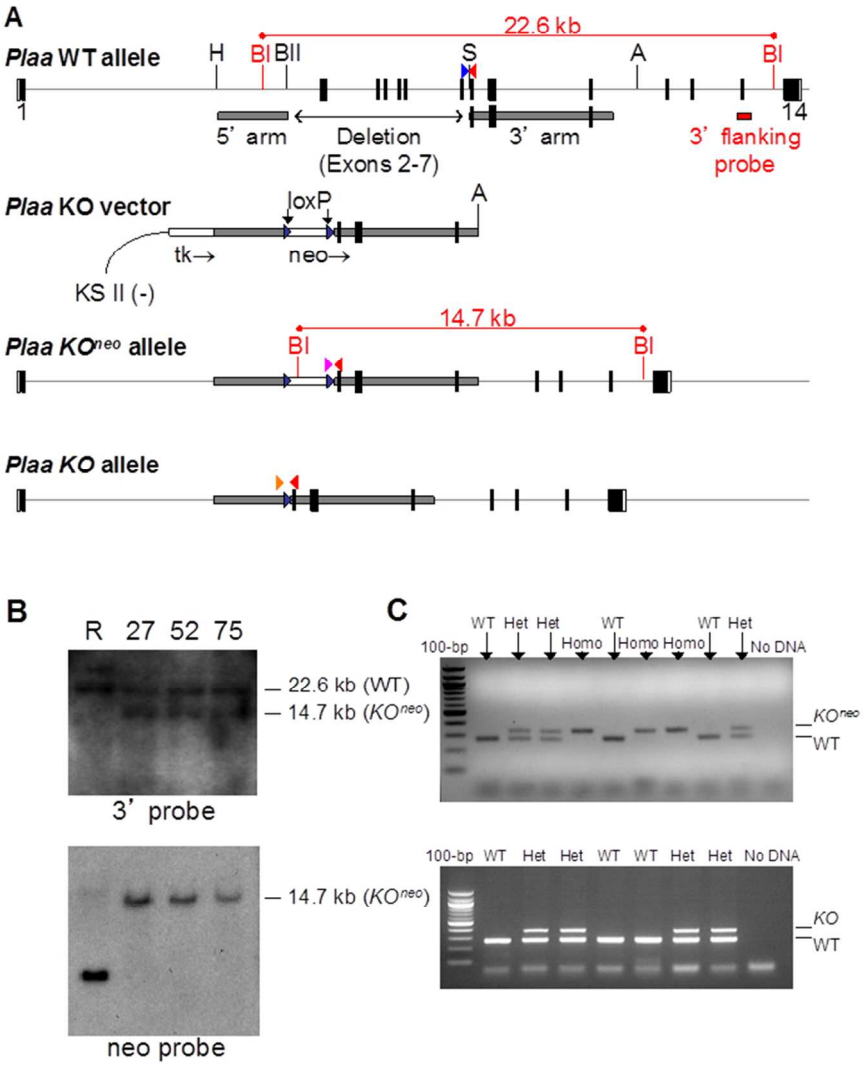

190x254mm (96 x 96 DPI)